Chemical Geology 353 (2013) 210–229

Contents lists available at ScienceDirect

Chemical Geology

journal homepage: www.elsevier.com/locate/chemgeo

Emplacement age and Sr–Nd isotopic compositions of the Afrikanda alkaline ultramafic complex, Kola Peninsula, Russia

Fu-Yuan Wu [a,*], Andrei A. Arzamastsev [b], Roger H. Mitchell [c], Qiu-Li Li [a], Jing Sun [a], Yue-Heng Yang [a], Ru-Cheng Wang [d]

[a] State Key Laboratory of Lithospheric Evolution, Institute of Geology and Geophysics, Chinese Academy of Sciences, P.O. Box 9825, Beijing 100029, China
[b] Geological Institute of the Kola Science Centre, Russian Academy of Sciences, Apatity, 184209, Russia
[c] Department of Geology, Lakehead University, Ontario, Canada P7B 5E1
[d] Department of Earth Sciences, Nanjing University, Nanjing 210093, China

ARTICLE INFO

Article history:
Accepted 13 September 2012
Available online 25 September 2012

Keywords:
U–Pb age
Nd–Sr isotopes
Perovskite
Titanite
Apatite
Afrikanda complex

ABSTRACT

The Kola Peninsula is characterized by diverse alkaline magmatism, including alkaline ultramafic, carbonatite, "kimberlite" and agpaitic rocks, although many aspects of the ages of emplacement and petrogenesis remain unresolved. In this study, rocks from the Afrikanda complex (pyroxenite, ijolite, melteigite, carbonatite, and perovskite ore) were selected for U–Pb age determination and Sr–Nd isotopic analyses using in situ ion probe and laser ablation techniques. The perovskite U–Pb ages are 377±6 (pyroxenite), 379±5 to 385±5 (calcite-bearing perovskite ore) and 376±5 (ijolite–melteigite) Ma, indicating that the different phases of the complex were contemporaneously emplaced at ~380 Ma. These ages are comparable to those obtained previously for Afrikanda rocks, and other alkaline ultramafic, carbonatitic, "kimberlitic" and agpaitic complexes in the area; suggesting that the majority of alkaline magmatism in the Kola Peninsula occurred at ~375–380 Ma. Sr–Nd isotopic analyses of perovskite, titanite, apatite, and calcite indicate that the Afrikanda complex was derived from a depleted mantle. However, these data suggest that silicate and carbonatitic magmas are not related by simple crystal fractionation within a closed magmatic system. The silicate magma has an initial $^{87}Sr/^{86}Sr$ isotopic ratio of ~0.7034 to 0.7038 and $\varepsilon_{Nd}(t)_{380}$ value of ~+2.0 to +4.9, whereas the carbonatitic magma was more primitive with the above values of ~0.7033 to 0.7035 and $\varepsilon_{Nd}(t)_{380}$ ~+5.1 to +5.8, suggesting that either both magmas were derived from two distinct mantle sources or by contamination of a melts derived from a single source. In combination with other geochronological and geochemical data for other complexes in the area, it is proposed that the Kola alkaline magmatism was controlled by mantle plume activity at ~380 Ma.

1. Introduction

Continental alkaline magmatism is represented by alkaline rocks that have higher concentration of alkalis than can be accommodated in feldspars alone, and characterized by the presence of feldspathoids, sodic pyroxene and amphibole, and other alkali-rich minerals (Sørensen, 1974). Although alkaline rocks account volumetrically for less than one percent of all igneous rocks, their remarkable diversities in mineralogy, petrology and geochemistry have made them the subject of many scientific studies during the past decades (Sørensen, 1974; Menzies, 1987; Mitchell, 2006; Tappe et al., 2007), mainly because these rocks can provide information regarding the composition and evolution of the continental lithospheric mantle. In addition, alkaline rocks are closely associated with many kinds of mineralization, and account for most of the world's resources of niobium, rare earth elements, phosphorus, zirconium and titanium.

Alkaline magmatism in the Kola Peninsula of Russia is represented by numerous Paleozoic (Devonian) intrusions, collectively termed the Kola Alkaline Province (KAP, Fig. 1). These intrusions have been classified as alkaline mafic–ultramafic rocks (turjaites, ijolites), agpaitic rocks (lujavrite), carbonatitic and rocks with "kimberlitic–lamproitic" affinities (some of the kimberlite-like rocks are actually lamprophyres, see Tappe et al. (2005)) (Downes et al., 2005). Current hypotheses for the petrogenesis of these rocks include derivation from a common primary magma by differentiation and/or liquid immiscibility, or from different batches of mantle melts (Harmer, 1999; Mitchell, 2005; Woolley and Kjarsgaard, 2008). For the Kola Alkaline Province, it has been proposed that the wide range of Sr–Nd isotopic compositions between the carbonatitic and silicate rocks suggested that they are not co-genetic, and the isotopic variation is a consequence of mixing of different batches of mantle-derived magma, but not from crustal

* Corresponding author. Tel.: +86 10 82998217; fax: +86 10 62010846.
E-mail address: wufuyuan@mail.igcas.ac.cn (F.-Y. Wu).

0009-2541/$ – see front matter © 2012 Elsevier B.V. All rights reserved.
http://dx.doi.org/10.1016/j.chemgeo.2012.09.027

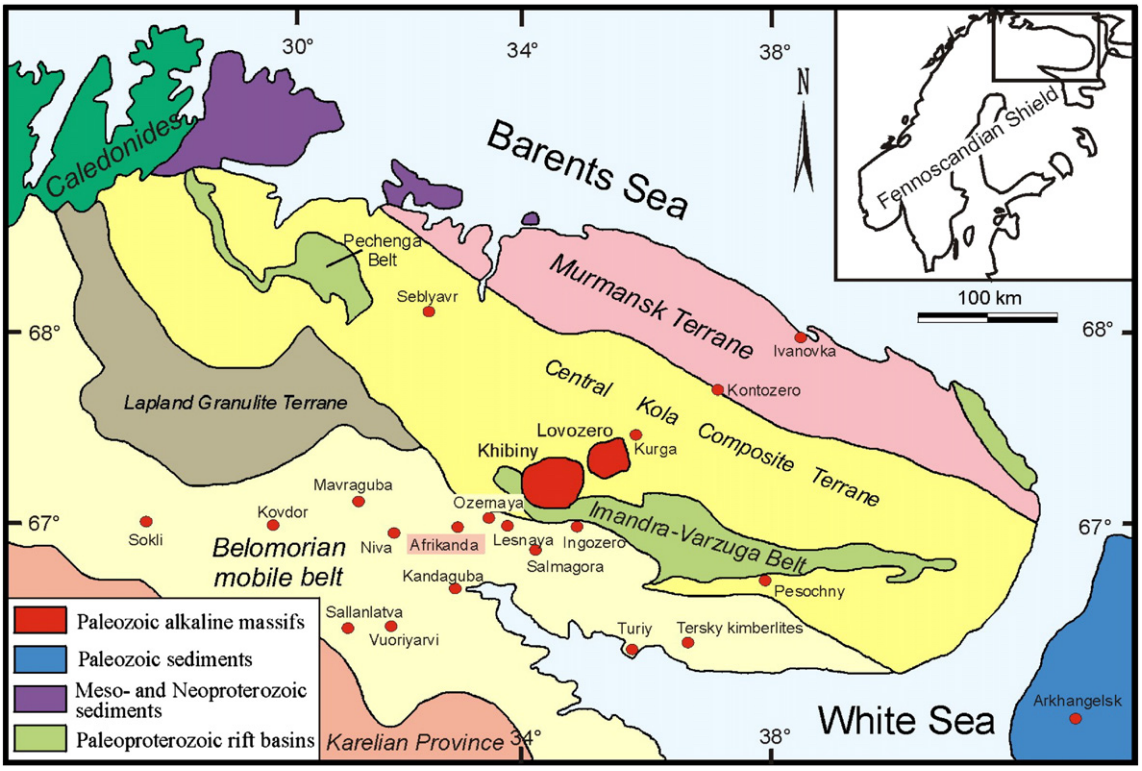

Fig. 1. Distribution map of the Paleozoic alkaline, ultramafic and "kimberlitic" intrusions of the Kola Peninsula. Tectonostratigraphic terrane subdivision is after Balagansky et al. (1998).

contamination because the carbonatites have extremely high Sr and Nd contents (Kramm, 1993; Kramm and Kogarko, 1994; Zaitsev and Bell, 1995; Verhulst et al., 2000; Dunworth and Bell, 2001; Zaitsev et al., 2002; Sindern et al., 2004; Lee et al., 2006). However, most carbonatites display uniform and identical Sr–Nd isotopic compositions to those of associated silicate rocks, thus favoring petrogenesis from a single batch of homogeneous mantle-derived melt that crystallized and fractioned in a closed system (Kogarko, 1987; Bell, 1996; Brassinnes et al., 2005; Balaganskaya et al., 2007; Bell and Simonetti, 2010). An alternative process is liquid immiscibility between a carbonatitic melt and an alkaline silicate melt (Ivanikov et al., 1998). Experimental work in the system of $CaO–Na_2O–(MgO+FeO)–(SiO_2+Al_2O_3)–CO_2$) shows that, depending on the system parameters (P, T, x), a miscibility gap can be reached during crystallization of a parental carbonated-silicate melt (Lee and Wyllie, 1998). However, typically there is no actual evidence for immiscibility in the generation of carbonatite from a carbonated silicate magma.

Another question concerning the petrogenesis of alkaline ultramafic igneous rocks is the nature of the mantle from which alkaline magmas are derived. Carbonatitic, agpaitic and lamproitic rocks are typically considered to be derived from the subcontinental lithosphere (Bell, 1996; Mitchell, 2006; Bell and Simonetti, 2010), although derivation from convecting mantle has been proposed (Bell and Blenkinsop, 1987, 1989; Simonetti and Bell, 1994a,b; Simonetti et al., 1997). It remains unknown as to why different mantle sources are partially melted coevally during a specific thermal event, how the magmas interact, and their subsequent evolution during magmatic crystallization.

To evaluate the above proposed genetic processes, it is necessary to assess the geochemical relationships between different contemporaneous rocks. For this purpose, the Afrikanda complex was selected for isotopic study as the occurrence consists of diverse rock types within a single intrusion.

2. Geological setting

The KAP, one of the largest alkaline — ultramafic–carbonatite provinces, is located in the Fennoscandian Shield and occupies an area of >100,000 km^2 (Fig. 1). In the northeastern part of this shield the Precambrian basement can be divided into three main units which are characterized by different times of continental crust formation. The Karelian Province and the Murmansk Terrane represent parts of the Early Archean cratons which are separated by the Lapland–Kola–Belomorian collision zone (Mitrofanov, 2001). All terranes and the Belomorian Belt had been involved and variably affected by Palaeoproterozoic collisional orogenesis, and show evidence of repetitive endogenic and exogenic processes which acted from the Archean to the Phanerozoic (Gorbatschev and Bogdanova, 1993). Most of the ultramafic, alkaline and carbonatite magmatism is located within this collision zone. The KAP is well-known not only for alkaline massifs, but also for melilitites, ultramafic lamprophyres and "kimberlites" (Downes et al., 2005). Of the 24 alkaline complexes presently identified, Khibiny and Lovozero are the two largest and composed of agpaitic nepheline syenites. Other complexes consist principally of alkaline ultramafic rocks with the majority containing carbonatite, e.g. the Kovdor, Vuoriyarvi, Salmagora, Seblyavr, Sallanlatva, Turiy Mys, Lesnaya, Ozernaya Ivanovka, and Afrikanda complexes (Fig. 2).

Afrikanda is located southwest of the Khibiny complex and is intrusive into Archean granitic gneisses and amphibolites. This circular complex has an exposed area of ~11.5 km^2 (Fig. 2) and is characterized by ultramafic, alkaline and carbonatitic rocks (Kogarko et al., 1995). Dunite (or olivinite) has been observed as enclaves within other rocks, indicating its early emplacement within the complex (1st phase). Pyroxenite (2nd phase) is the dominant rock type occupying >90 vol.% of the exposed area (Fig. 2). The marginal near-contact pyroxenite and apophyses are feldspar-bearing, whereas towards the center of the complex

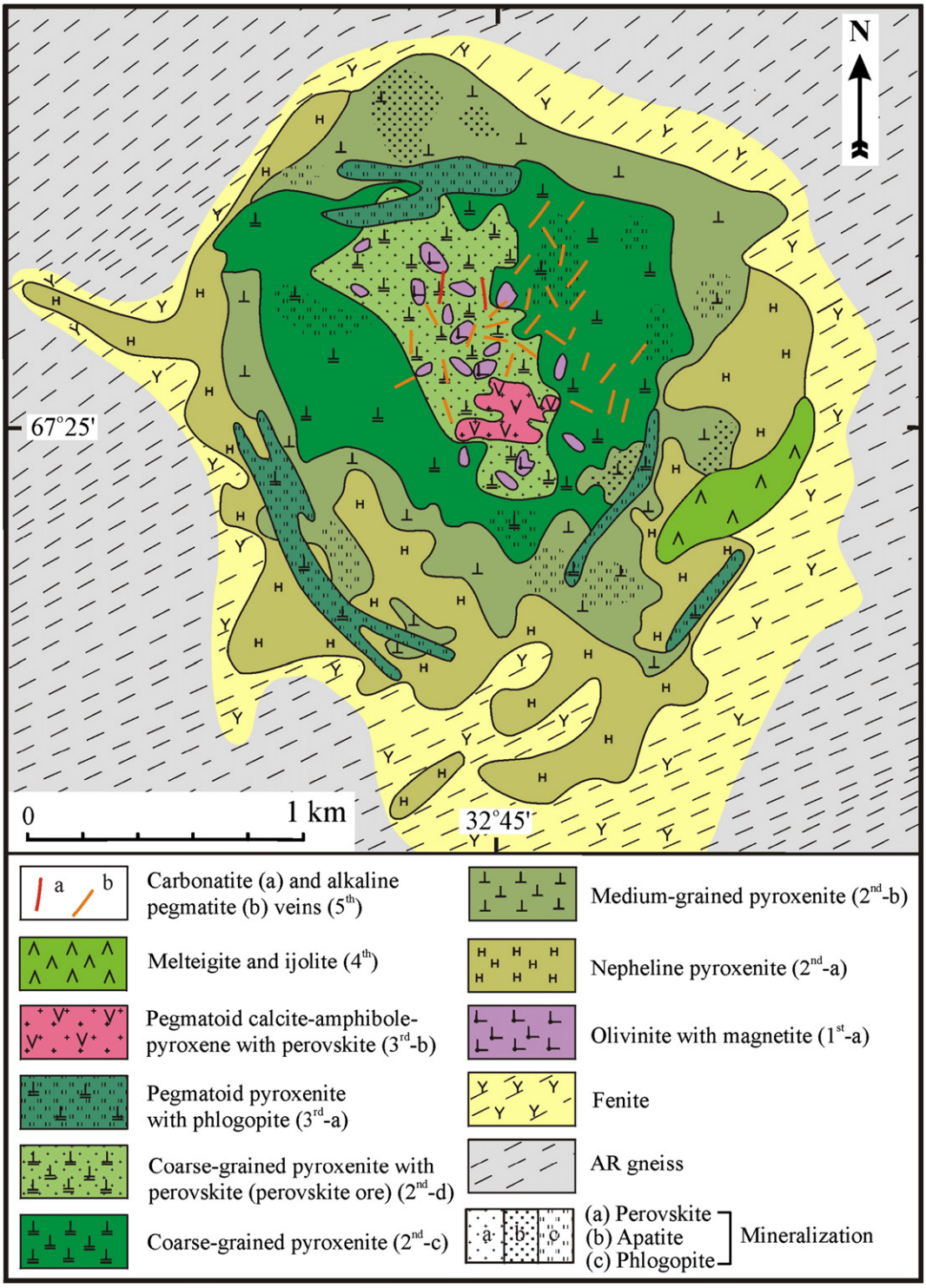

Fig. 2. Geological map of the Afrikanda complex.
Modified from Kukharenko et al. (1965) and Pozhilenko et al. (2002).

the pyroxenite grades into nepheline-bearing coarse-grained varieties. Pyroxenite commonly exhibits igneous layering manifested as alternating bands of oxide and silicate minerals. The central part, usually classified as pegmatitic pyroxenite (3rd phase), has a complicated structure and assemblage; including pyroxenite, calcite–amphibole–diopside rock, alkaline pegmatite, titanite-bearing carbonatite and perovskite–phlogopite–titanomagnetite veins. The rocks of the foidolite series form a single body southeast of the center of the massif (4th phase). These consist dominately of fine-grained melteigite with nepheline-rich ijolite layers. The latter also occur sporadically in veins. According to Chakhmouradian and Zaitsev (2004), ijolite–melteigite cross-cut the ultramafic and pegmatoid calcite-bearing rocks. The final intrusions include carbonatitic and alkaline pegmatitic dykes (5th phase, Fig. 2).

Although the Afrikanda complex is well known for its geology and mineralogy together with the mineral resources (Kukharenko et al., 1965; Chakhmouradian and Mitchell, 1997; Chakhmouradian

and Zaitsev, 1999, 2002; Zaitsev and Chakhmouradian, 2002; Chakhmouradian, 2004; Chakhmouradian and Zaitsev, 2004; Chakhmouradian and Williams, 2004), it has been less studied with respect to its age and isotopic composition. The Afrikanda complex has also provided material for studies of the U–Pb and trace element geochemistry of calzirtite and zirconolite (Williams and Gieré, 1996; Williams et al., 2001; Chakhmouradian and Williams, 2004; Bulakh et al., 2006; Wu et al., 2010c). An emplacement age of 364.0 ± 3.1 Ma was obtained from a mineral Rb–Sr isochron for a pyroxenite (AF-7994), with an initial Sr isotopic ratio of 0.7032 ± 1 (Kramm et al., 1993). However, recent studies using the perovskite U–Pb system indicate that this complex was emplaced at around 380 Ma (Reguir et al., 2010; Wu et al., 2010c). The reason for the younger age obtained by Kramm et al. (1993) is probably the lower closure temperature of the Rb–Sr system compared to that of perovskite U–Pb isotopic systems. Wu et al. (2010c) have reported that the Afrikanda complex has an initial Sr isotopic ratio of 0.7032–0.7033 and $\varepsilon_{Nd}(t)_{380}$ value of +5.5 to +6.2 by analyzing minerals from calzirtite- and zirconolite-bearing pyroxenite.

In this study, sixteen samples were collected for comprehensive U–Pb age determination and Sr–Nd isotopic analysis (Table 1). For the main phase of pyroxenite (2nd phase), two medium- to coarse-grained pyroxenites were selected: samples 25-AF (medium-grained) and 10AFK3 (coarse-grained). These samples have similar mineral assemblages of clinopyroxene, olivine, magnetite, apatite, amphibole, phlogopite, titanomagnetite and perovskite (Fig. 3a). Eight samples collected from the irregular pegmatoid bodies (3rd phase), including pegmatitic pyroxenite and calcite–amphibole–pyroxene rock, in the inner part of the complex are perovskite ore with minor and variable amounts of titanite (<5 vol.%), apatite (<5 vol.%) and calcite (<10 vol.%), distributed interstitially between pyroxene and perovskite (Fig. 3b and c). The exception is sample 10AFK5 which contains up to ~40 vol.% calcite in addition to perovskite, pyroxene, amphibole, titanite and ilmenite (Fig. 3d). In these samples, the grain-size of perovskite exhibits a large variation, from less than 0.1 mm to greater than 20 mm (Fig. 3c and d). Six samples collected from the 4th phase of the complex are fine-to-medium grained melteigite and ijolite with clinopyroxene (60–90 vol.%), nepheline (10–40 vol.%), phlogopite (5–10 vol.%), magnetite (<5 vol.%) and garnet (schorlomite, 0–5 vol.%) as the main components with accessory apatite, titanite and perovskite (Fig. 3e and f). Samples P07-23 and P07-24 do not contain perovskite, and P07-24 contains melilite (20–30 vol.%). No samples were collected for the 1st and 5th phases of olivinite and carbonatitic/alkaline pegmatitic dykes, due to their limited occurrence.

Table 1
Sample list and the analyzed minerals.

Phase	Rock type	Sample	Analyzed minerals
1st	Olivinite		
2nd (a)	Nepheline pyroxenite		
2nd (b)	Medium-grained pyroxenite	25-AF	Prv, Ap, Tit
2nd (c)	Coarse-grained pyroxenite	10AFK3	Prv, Ap, Tit
3rd	Perovskite ore	AFK	Prv, Tit, Cc
3rd	Perovskite ore	AFK-1	Prv, Ap, Tit, Cc
3rd	Perovskite ore	AFK-2	Prv, Tit, Cc
3rd	Perovskite ore	AFK-5	Prv, Cc
3rd	Perovskite ore	10AFK1	Prv, Cc
3rd	Perovskite ore	10AFK2	Prv, Cc
3rd	Perovskite ore	10AFK4	Prv, Ap, Tit, Cc
3rd	Perovskite ore	10AFK5	Prv, Tit, Cc
4th (a)	Fine-grained melteigite	P07-21	Prv, Ap
4th (a)	Fine-grained melteigite	P07-22	Ap
4th (a)	Fine-grained melteigite	P07-25	Ap
4th (a)	Fine-grained melteigite	P07-26	Prv, Ap, Tit
4th (b)	Fine-grained ijolite	P07-23	Ap
4th (b)	Medium-grained ijolite	P07-24	Ap
5th	Carbonatite/alkaline pegamatite		

Note: Prv: perovskite; Ap: apatite; Tit: titanite; Cc: calcite.

3. Analytical methods

Separated mineral grains of perovskite, apatite, titanite and calcite were handpicked, mounted in epoxy resin, and polished until the grain centers of the grains were exposed. Before isotopic analysis, back-scattered electron (BSE) images were obtained using a JEOL JXA8100 electron microprobe, in order to assess internal compositional variation and textures, and identify potential target sites for U–Pb and Sr–Nd analyses. All analyses were conducted at the Institute of Geology and Geophysics, Chinese Academy of Sciences.

3.1. Major and trace element analyses

Major element compositions were obtained using a JEOL-JAX8100 electron microprobe with a 15 kV accelerating potential and a 12 nA beam current. Counting times were 20 s. Total iron is expressed as FeO. The analytical uncertainties are within 2% for TiO_2 and CaO, but ~10–20% for other elements due to their low concentrations.

Trace element compositions (including REE) were conducted using an Agilent 7500a Q-ICP-MS (quadruple inductively coupled plasma mass spectrometry), which is equipped with a 193 nm excimer ArF laser-ablation system (GeoLas Plus). Helium gas was flushed to minimize aerosol deposition around the ablation site, and mixed with argon gas downstream of the ablation cell. During analyses, a spot size of 30 μm was applied with a repetition rate of 6 Hz. Each of the five sample analyses was followed by one NIST SRM 610 measurement. Each spot analysis consisted approximately of 30s of background acquisition and 60s of sample data acquisition. Trace element concentrations were calculated using GLITTER 4.0 and calibrated using ^{40}Ca as an internal standard and NIST610 as an external reference material (Jackson et al., 2004; Griffin et al., 2008).

3.2. In situ U–Pb analyses of perovskite by SIMS

The U–Pb analyses of this study in part undertaken using the CAMECA1280 ion microprobe installed at the Institute of Geology and Geophysics in Beijing. The instrument description and analytical procedure can be found in Li et al. (2009, 2010), and only a brief summary is given here. The O_2^- primary ion beam was accelerated at 13 kV, with intensity between 10 and 18 nA. The analyzed ellipsoidal spot size is about 20 × 30 μm in size. Positive secondary ions were extracted with a 10 kV potential.

All samples analyzed in this study were cast in epoxy mounts. Each mount was coated with about 30 nm of high-purity gold to reach <20 Ω resistance. Sample charging effects were minimized by optimizing the energy offset to maximum transmission in the 60 eV energy window at the start of each analysis using the $^{40}Ca^{48}Ti_2^{16}O_4$ reference peak at mass 200. This peak of $^{40}Ca^{48}Ti_2^{16}O_4$ is a matrix reference for centering the secondary ion beam, energy and mass adjustments, as well as reference for mass 200.5 (background). The field aperture was set to 5000 μm, and the transfer optic magnification was adjusted to 200 with Max Area of 40 μm. Rectangular lenses were activated in the secondary ion optics to increase the transmission at high mass resolution. A mass resolution of ca. 8000 (defined at 50% peak height) was used to separate $^{40}Ca^{48}Ti_2^{16}O_4^+$ peaks from isobaric interferences. This mass resolution is enough to separate U, Th and Pb isotopes from isobaric interferences, such as oxides of the REE (e.g., Williams, 1998). A single electron multiplier was used in ion-counting mode to measure secondary ion beam intensities by peak jumping. Each measurement consists of 10 cycles, and the total analytical time was ca. 16 min. The mass fractionation of Pb isotopes and interferences from Pb hydrides (requiring a mass resolution > 30,000) were not considered

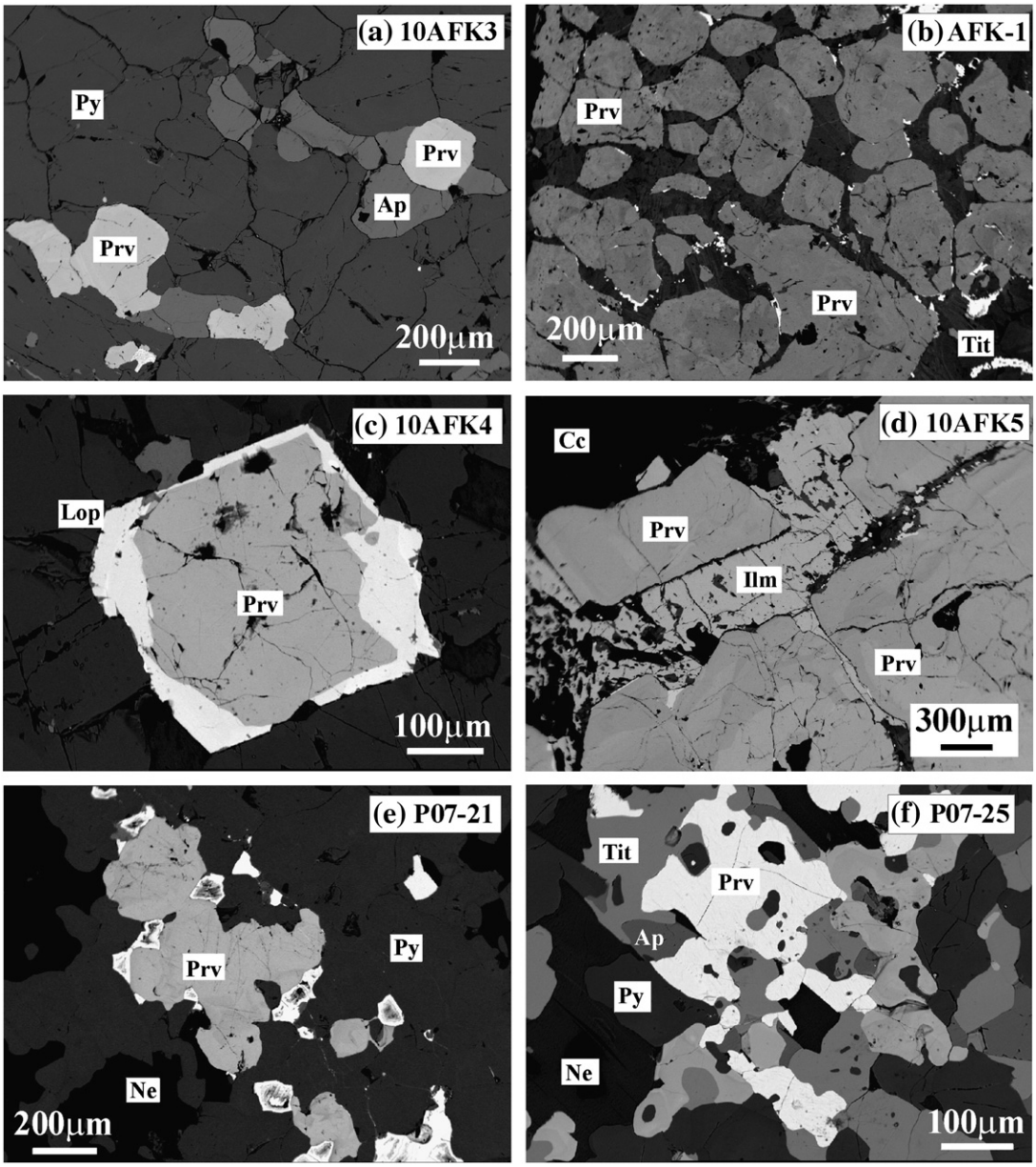

Fig. 3. Petrographic characters of the samples investigated showing the occurrence of perovskite. Prv: perovskite; Py: clinopyroxene; Ap: apatite; Lop: loparite; Tit: titanite; Cc: calcite; Ilm: ilmenite; Ne: nepheline.

because previous studies have shown that these two effects are negligible and there appears to be a mutual cancelation (Li et al., 2009, 2010).

During analyses, Ice River perovskite served as the primary standard and was measured after every three unknown perovskite grains. However, note that an average $^{206}Pb/^{238}U$ age of 356.5 ± 1.0 Ma for the Ice River perovskite was applied for calibration of our data (Heaman, 2009), whereas a revised age of 361.7 ± 1.0 Ma is given by Tappe and Simonetti (2012). The Tera-Wasserburg diagram was used to give a lower intercept, the crystallization age of the analyzed mineral, assuming the common lead is controlled by the model of Stacey and Kramers (1975). The ^{207}Pb correction method was used for the individual analysis, and then an average $^{206}Pb/^{238}U$ age with 2σ or 95% confidence level was calculated using ISOPLOT 3.0 (Ludwig, 2003).

To check the reliability of our technique and the common lead composition, perovskite from sample AFK was analyzed by isotopic dilution methods (Table 2a), and a lower intercept age of 379.6 ± 9.9 Ma was obtained from four analyses (Fig. 4a), with a ^{207}Pb corrected age of 378.6 ± 4.1 Ma (Fig. 4a). If the ^{204}Pb correction is applied, the obtained weighted $^{206}Pb/^{238}U$ age is 381.6 ± 1.4 Ma, identical within error to that obtained by ^{207}Pb correction (Fig. 4b). For SIMS analyses, thirty-eight analyses of AFK give a lower intercept age of 385 ± 15 Ma with a ^{207}Pb corrected age of 383.5 ± 3.5 Ma (Fig. 4c). Similarly, the ^{204}Pb corrected age is 382.8 ± 3.6 Ma (Fig. 4d). In addition, analyses of Tazheran perovskite yielded intercept, ^{207}Pb and ^{204}Pb corrected ages of 467 ± 5, 467 ± 4 and 467 ± 4 Ma (Fig. 4e and f), respectively, consistent with the recommended value (463 ± 2 Ma) obtained by TIMS analyses (Oversby and Ringwood, 1981; Kinny et al., 1997). The above consistency indicates that both the analytical technique and the common lead composition we applied are reliable for obtaining accurate U–Pb ages for the perovskites investigated.

Table 2
TIMS U–Pb (a), Rb–Sr (b) and Sm–Nd (c) isotopic data of the AFK in-house perovskite standard.

(a) U–Pb isotopes

Sample	U (ppm)	Pb (ppm)	Th (ppm)	Th/U	$^{206}Pb/^{204}Pb$	Isotopic ratio uncorrected			
						$^{238}U/^{206}Pb$	2σ (%)	$^{207}Pb/^{206}Pb$	2σ (%)
AFK A	77.2	17	632	8.4	155	14.6716	0.52	0.1438	2.10
AFK B	112.0	25.6	895	8.2	132	14.2276	0.13	0.1631	0.93
AFK C	107.6	31.7	1358	13.0	87	12.9932	0.14	0.2197	0.48
AFK D	121.8	25.8	942	7.9	126	14.0488	0.12	0.1684	0.39

Sample	Isotopic data (^{204}Pb corrected)						Isotopic age (Ma)		
	$^{207}Pb/^{235}U$	2σ (%)	$^{206}Pb/^{238}U$	2σ (%)	$^{207}Pb/^{206}U$	2σ (%)	$^{206}Pb/^{238}U$	$^{206}Pb/^{235}U$	$^{206}Pb/^{238}U$
AFK A	0.4529	1.94	0.0606	0.52	0.0542	1.85	379.2 ± 2.0	379.3 ± 7.4	379.6 ± 41.5
AFK B	0.4576	0.90	0.0608	0.13	0.0546	0.83	380.7 ± 0.5	382.6 ± 3.4	394.1 ± 18.6
AFK C	0.4461	1.17	0.0611	0.14	0.0530	1.07	382.2 ± 0.5	374.6 ± 4.4	327.4 ± 24.4
AFK D	0.4503	0.73	0.0611	0.12	0.0535	0.66	382.0 ± 0.4	377.5 ± 2.8	350.0 ± 15.0

$^{206}Pb/^{238}U$ weighted average age: 381.6 ± 1.4 Ma (2σ).

(b) Rb–Sr isotopes

Sample	Rb (ppm)	Sr (ppm)	$^{87}Rb/^{86}Sr$	$^{87}Sr/^{86}Sr$	2σ
AFK-a	1.95	2441	0.0023	0.703320	0.000012
AFK-a (replicate)		2441		0.703335	0.000011
AFK-b	1.19	2563	0.0013	0.703359	0.000012
AFK-b (replicate)		2563		0.703370	0.000011
AFK-c	2.83	2404	0.0034	0.703352	0.000013

$^{87}Sr/^{86}Sr$ weighted average ratio: 0.703347 ± 39 (2SD)

(c) Sm–Nd isotopes

Sample	Sm (ppm)	Nd (ppm)	$^{147}Sm/^{144}Nd$	$^{143}Nd/^{144}Nd$	2σ
AFK-a	835	7844	0.0644	0.512594	0.000004
AFK-a (replicate)				0.512592	0.000008
AFK-b	890	8110	0.0663	0.512627	0.000009
AFK-b (replicate)				0.512619	0.000010
AFK-c	849	7659	0.0670	0.512607	0.000009
AFK-C (replicate)				0.512614	0.000009

$^{147}Smr/^{144}Nd$ and $^{143}Ndr/^{144}Nd$ weighted average ratios: 0.0659 and 0.512609 ± 27 (2SD).

3.3. In situ U–Pb analyses of perovskite by laser ablation

Some perovskite U–Pb age determinations were conducted using an Agilent 7500a ICP–MS. The analytical details can be found in Yang et al. (2009) and Wu et al. (2010a). During laser ablation, the applied spot size is 40 μm with a laser repetition of 10 Hz and laser energy density of 15 J/cm^2. The background of ^{204}Pb and ^{202}Hg was less than 100 cps because of the high purity of the argon and helium that was used. ICP–MS measurements were carried out using time-resolved analysis and peak hopping at one point per mass. Each of the five-sample analyses was followed by one Tazheran standard perovskite and one NIST SRM 610 measurement. Each spot analysis consisted approximately of 30s background acquisition and 40s sample data acquisition. The fractionation correction and results were calculated using GLITTER 4.0 (GEMOC, Macquarie University). For this type of ICP–MS analysis, the ^{204}Pb contents cannot be precisely determined due to interference from a ^{204}Hg contaminant in the carrier gases. Therefore, a ^{207}Pb but not a ^{204}Pb correction was applied for the age calculation, in addition to the intercept age obtained from the Tera–Wasserburg U–Pb diagram.

3.4. In situ Sr–Nd isotopic analyses by laser ablation

The in situ Sr–Nd isotopic analyses were conducted using a Neptune MC-ICP-MS instrument. Detailed analytical protocols are given by Xie et al. (2008), Yang et al. (2008, 2009) and Wu et al. (2006), only a brief summary is given here.

The Sr isotopic data were acquired in static, multi-collector mode with low resolution using eight Faraday collectors, and the mass configuration array from ^{83}Kr to ^{88}Sr, monitoring Kr and Rb (Yang et al., 2009). Prior to analysis, collectors were aligned using a tuning solution which contains Rb, Sr, Er, and Yb. An aliquot of 200 ppb NIST 987 standard was used regularly for controlling the quality and optimizing the operation parameters, including the torch position, the Ar flow rate, and the ion lens focus, to obtain maximum sensitivity. During the data reduction process, the effects of interfering elements were accounted for in the order Kr, Yb^{2+}, Er^{2+} and Rb, but interferences from Fe dioxides, and Ga and Zn oxides, are not considered due to their low signals during actual analyses. Similarly, no corrections for $^{176}Lu^{2+}$ and $^{176}Hf^{2+}$ on ^{88}Sr were considered as their interferences on ^{88}Sr are negligible. Prior to every analytical session, the Neptune MC-ICP-MS was always configured to monitor Kr in the Ar gas after optimization, especially when a new liquid Ar tank was replaced. During analyses, a 50 second measurement of the gas blank was carried out before ablation in order to correct for Kr. Based on the method proposed by Ramos et al. (2004), we monitored the presence of $^{167}Er^{2+}$, $^{171}Yb^{2+}$ and $^{173}Yb^{2+}$ at masses 83.5, 85.5 and 86.5. Then the contributions of $^{168}Er^{2+}$ and $^{168}Yb^{2+}$ to ^{84}Sr, $^{170}Er^{2+}$ and $^{170}Yb^{2+}$ to ^{85}Sr (+^{85}Rb), $^{172}Yb^{2+}$ to ^{86}Sr, $^{174}Yb^{2+}$ to ^{87}Sr (+^{87}Rb), and $^{176}Yb^{2+}$ to ^{88}Sr were calculated according to the isotopic abundances of Er and Yb (Chartier et al., 1999; Vervoort et al., 2004). The natural ratio of $^{85}Rb/^{87}Rb$ (2.5926) was used for isobaric correction of Rb by the exponential law, assuming that rubidium has the same mass discrimination as strontium (Ehrlich et al., 2001). In order to avoid matrix-mismatch effects, an in-house perovskite (AFK)

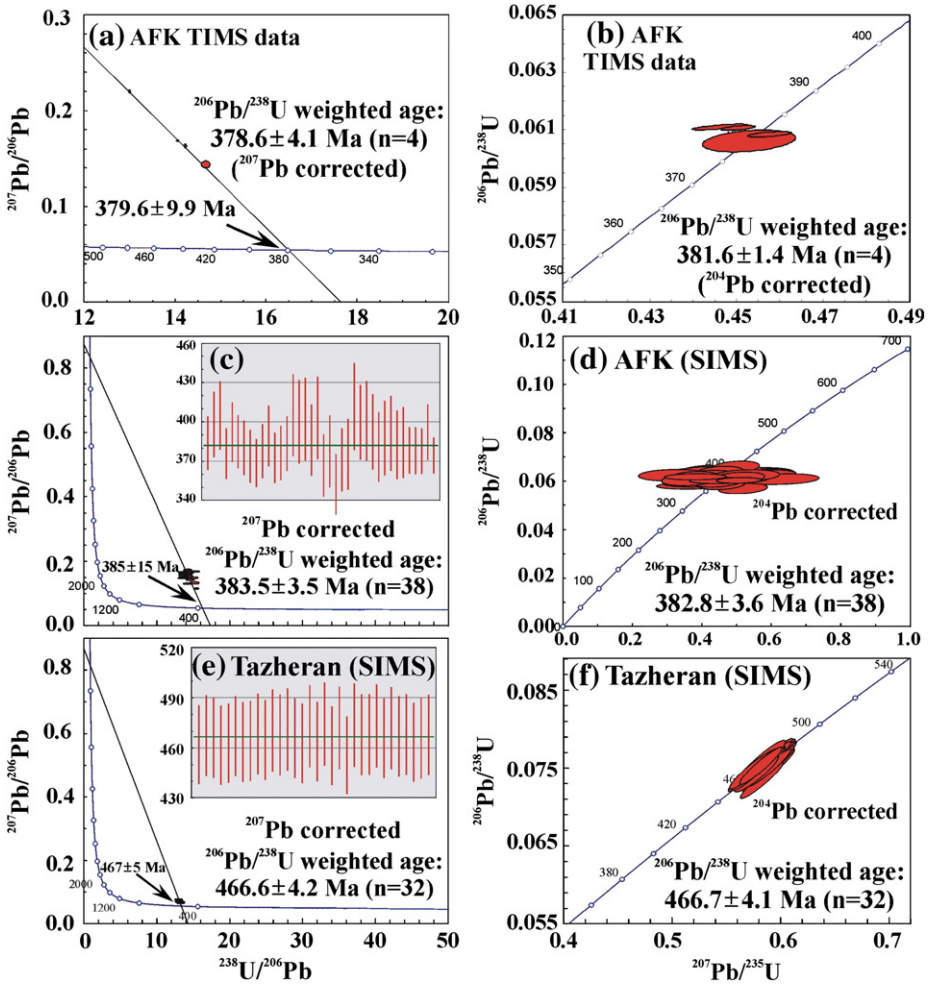

Fig. 4. U–Pb age determinations of standard perovskites.

standard was used for the external correction of $^{87}Sr/^{86}Sr$ ratio. However, no $^{87}Rb/^{86}Sr$ ratio is corrected since this ratio is extremely low, and has no effect on the initial $^{87}Sr/^{86}Sr$ ratio of the sample studied as demonstrated by Wu et al. (2010c). Five TIMS analyses produced a weighted mean $^{87}Sr/^{86}Sr$ ratio of 0.70335±4 (n=5, 2SD) with $^{87}Rb/^{86}Sr$ ratio ranging from 0.0013 to 0.0034 (Table 2b). However, the $^{87}Rb/^{86}Sr$ ratio (0.00008) of AFK by laser ablation is much lower than that (0.00141) obtained by TIMS analyses. The difference is ascribed to the presence of Rb in fractures in the perovskite. This material cannot be eliminated in bulk TIMS analyses.

The laser ablation Nd isotope technique is similar to that for Sr isotope analysis as described above. Before analysis, a standard Nd solution was used to calibrate the machine and the exponential law was applied for mass bias correction assuming $^{146}Nd/^{144}Nd=0.7219$. During laser analyses, the interferences are caused principally by Ce (^{142}Ce on ^{142}Nd) and Sm (^{144}Sm on ^{144}Nd). However, our work indicates that the influence of Ce on Nd isotope analysis is insignificant (Yang et al., 2008), although much attention has to be given to the isobaric interference of ^{144}Sm on ^{144}Nd (McFarlane and McCulloch, 2007). In this study, the mass bias of Sm (β_{Sm}) was directly obtained from the $^{147}Sm/^{149}Sm$ ratio on the sample itself and then applied in the isobaric interference correction following the method proposed by McFarlane and McCulloch (2007) assuming $^{147}Sm/^{149}Sm=1.08680$ (Dubois et al., 1992) and $^{144}Sm/^{149}Sm=0.22332$ (Isnard et al., 2005). Further, $^{145}Nd/^{144}Nd$ ratio was used to evaluate the feasibility of our method as it has a constant value of 0.348415 (Wasserburg et al., 1981). As proposed by recent studies (Fisher et al., 2011; Iizuka et al., 2011), an in-house perovskite standard (AFK) was used for the external corrections of $^{147}Sm/^{144}Nd$ and $^{143}Nd/^{144}Nd$ in order to overcome the potential matrix-mismatch effects. Six TIMS analyses gave a weighted mean $^{143}Nd/^{144}Nd$ ratio of 0.512609±27 (n=6, 2SD) with a $^{147}Sm/^{144}Nd$ ratio of 0.0659 (Table 2c). During this study, fifty-eight analyses of AFK yielded a variation of $^{147}Sm/^{144}Nd$ of 4.1% (2RSD), which results in a 0.1 ε_{Nd} variation if assuming an age of 380 Ma, indicating that the small heterogeneity of the AFK $^{147}Sm/^{144}Nd$ ratio has no significant effect on the ε_{Nd} values of the Afrikanda samples.

4. Analytical results

4.1. Mineral compositions

In this study, sixteen samples were selected for analysis (Table 1). Their compositions are listed in Table 3 and the rare earth element (REE) distribution patterns are shown in Fig. 5. Of these samples, most are euhedral perovskite with a grain-size of ~200 μm (Fig. 3). Some perovskites are mantled by later-crystallizing loparite (Fig. 3c). From these data, the perovskites can be seen to have similar compositions to those occurring in kimberlites (Chakhmouradian and Mitchell, 2001a, 2001b), in consisting mainly of TiO_2 (53.3–57.6 wt.%) and CaO (35.7–39.2 wt.%) with minor Fe_2O_3 (0.7–1.6 wt.%) and Na_2O

Table 3
Chemical compositions of the analyzed minerals (major elements: wt.%; trace elements: ppm).

Sample	25-AF	10AFK3	AFK	AFK-1	AFK-2	AFK-5	10AFK1	10AFK2	10AFK4	10AFK5	P07-21	P07-26	25-AF	10AFK3	AFK-1	10AFK4	P07-21	P07-22	P07-23
Mineral	Prv	Prv	Prv	Prv	Prv	Prv	Prv	Prv	Prv	Prv	Prv	Prv	Ap	Ap	Ap	Ap	Ap	Ap	Ap
SiO_2													0.61	0.35	0.14	0.70	0.59	0.80	0.60
TiO_2	57.33	56.33	54.00	53.34	53.87	54.16	57.41	55.66	55.83	55.78	56.76	57.57							
Al_2O_3	0.10	0.15	0.19	0.17	0.17	0.16	0.12	0.18	0.14	0.19	0.09	0.05							
FeO	0.93	1.18	1.64	1.56	1.50	1.47	0.97	1.35	1.16	1.36	0.92	0.68							
CaO	38.81	37.26	35.70	36.65	36.65	37.33	38.89	37.29	36.73	36.81	37.15	39.17	54.75	52.99	53.27	54.68	54.26	54.51	54.23
Na_2O	0.37	0.57	0.93	0.79	0.83	0.72	0.38	0.58	0.73	0.58	0.77	0.51		0.16	0.23				
P_2O_5													40.88	40.83	41.98	40.37	40.79	40.60	40.79
Total	97.54	95.49	92.46	92.51	93.02	93.84	97.77	95.06	94.59	94.72	95.69	97.98	96.24	94.33	95.62	95.75	95.64	95.91	95.62
Rb	0.18	0.16	0.65	0.45	0.42	0.41	0.21	0.22	0.13	0.13	0.20	0.16	0.25	0.24	0.23	0.26	0.27	0.24	0.28
Sr	3569	3014	3087	2776	2765	2783	2536	2792	2362	2421	3480	2184	5226	4177	4611	4273	7107	5751	6206
Ba	2.8	1.4	2.0	1.4	1.7	1.5	1.2	2.6	1.2	1.3	1.8	5.0	19	7.3	19	14	20	18	17
Nb	6003	7567	13,240	8493	9192	8762	5115	6729	7584	8034	9373	10,049	0.27	0.37	112	0.14	0.30	0.77	0.93
Ta	221	366	687	383	390	358	301	307	293	305	449	352	0.05	0.05	6.7	0.05	0.05	0.05	0.05
Zr	147	139	390	285	301	297	284	263	211	299	151	207	3.7	10	73	0.66	7.0	11	11
Hf	5.4	4.4	7.9	6.2	6.2	5.8	8.9	8.5	5.2	7.1	3.4	4.7	0.28	0.29	1.7	0.30	0.30	0.29	0.32
Pb	14	25	43	68	37	33	20	22	23	27	16	14	1.7	1.1	9.0	2.1	1.5	1.9	2.2
Th	192	851	2038	1003	1118	905	593	614	602	794	328	92	18	12	12	38	36	50	35
U	69	86	185	179	164	163	74	80	121	126	75	177	3.4	1.5	0.72	1.3	3.7	7.0	5.3
La	5988	8276	12,069	9770	10,007	10,162	7214	8579	8253	9127	6616	1744	1435	1028	3252	3000	1302	1950	1841
Ce	9313	17,314	29,262	21,637	22,653	21,824	13,779	16,963	17,234	20,155	14,991	4568	1811	1568	6818	6437	2078	3250	3171
Pr	832	1714	3356	2245	2380	2228	1385	1686	1740	2074	1620	616	156	158	866	752	207	330	328
Nd	2665	5660	11,096	7637	8199	7463	4608	5582	5832	7077	5607	2597	394	454	3486	2837	666	1108	1096
Sm	368	630	1051	840	907	824	534	629	648	794	662	439	76	86	545	371	92	129	130
Eu	112	159	231	201	217	200	143	162	158	187	162	122	22	23	142	84	23	31	30
Gd	228	310	468	380	417	382	277	305	309	368	323	266	65	72	326	212	68	82	82
Tb	24	30	43	36	40	36	28	29	29	34	33	27	7.2	7.9	32	20	7.1	7.7	7.7
Dy	93	114	169	132	142	128	106	106	108	126	132	107	31	36	118	72	31	31	30
Ho	12	15	21	16	17	16	15	13	13	15	17	14	5.0	5.8	15	9.4	5.1	4.5	4.4
Er	19	24	34	27	28	25	25	21	22	25	31	25	8.9	10.8	26	14.2	9.4	7.8	7.5
Tm	1.5	1.9	2.7	2.2	2.2	1.9	2.1	1.6	1.7	1.9	2.6	2.1	0.87	1.1	2.2	1.2	0.98	0.79	0.74
Yb	6.6	8.2	11	9.4	8.8	8.3	9.8	7.0	7.7	8.5	12	11	4.3	6.0	9.3	5.3	5.2	4.1	3.7
Lu	0.56	0.68	0.92	0.72	0.72	0.70	0.84	0.56	0.62	0.69	1.0	0.88	0.46	0.68	0.98	0.46	0.60	0.48	0.40
Y	162	199	302	246	252	236	226	171	210	222	252	253	95	120	262	138	106	95	96

(*continued on next page*)

Table 3 (*continued*)

Sample	P07-24	P07-25	P07-26	25-AF	10AFK3	AFK	AFK-1	AFK-2	10AFK-4	P07-26	10AFK5	AFK	AFK-1	AFK-2	AFK-5	10AFK1	10AFK2	10AFK4	10AFK5
Mineral	Ap	Ap	Ap	Tit	Tit	Tit	Tit	Tit	Tit	Tit	Tit	Cc	Cc	Cc	Cc	Cc	Cc	Cc	Cc
SiO_2	0.68	0.79	0.54	30.97	31.08	30.95	31.02	31.22	31.10	30.98	31.12								
TiO_2				37.69	37.34	35.30	31.80	33.56	38.55	37.67	38.96								
Al_2O_3				1.04	1.21	0.82	3.83	2.48	0.23	0.91	0.20								
FeO				1.36	1.12	2.26	1.37	2.51	1.19	1.21	1.01								
CaO	54.62	54.82	54.69	28.23	27.99	27.89	28.59	28.76	27.66	28.25	27.52								
Na_2O							0.09	0.05	0.23	0.05	0.23								
P_2O_5	41.04	40.56	40.95																
Total	96.34	96.17	96.18	99.29	98.74	97.22	96.70	98.58	98.96	99.07	99.04								
Rb	0.27	0.29	0.26	0.23	0.34	0.31	0.05	0.28	0.38		0.33	0.27	0.08	0.06	0.06	0.32	0.26	0.32	0.29
Sr	5430	4789	4666	608	335	321	494	779	482		426	2997	2967	2576	930	3447	1971	6542	5407
Ba	13	9.9	34	1.1	1.4	4.8	3.0	380	1.4		18	69	240	171	95	1250	521	733	153
Nb	0.91	1.29	0.52	1992	2918	4148	5396	6156	4168		3535	0.19	0.08	0.27	0.76	0.30	0.46	0.15	0.14
Ta	0.05	0.05	0.05	61	185	220	309	278	170		170	0.06	0.00	0.02	0.02	0.07	0.06	0.06	0.05
Zr	9.1	10	6.4	1709	2342	2534	2231	151	2906		2686	0.41	0.14	0.08	8.6	0.49	0.40	0.45	0.43
Hf	0.31	0.32	0.30	52	60	39	48	3.6	48		41.55	0.33	0.03	0.02	0.21	0.36	0.32	0.35	0.34
Pb	2.6	1.2	1.3	1.6	3.5	2.0	3.5	12	1.1		0.93	0.88	0.78	1.3	1.7	0.69	1.01	3.9	1.61
Th	30	28	36	7.9	133	42	43	53	24.77		22.10	0.14	0.04	0.22	0.45	0.26	0.08	0.05	0.05
U	4.6	3.9	5.2	4.0	14	13	2.6	78	1.5		2.75	0.05	0.02	0.01	0.06	0.05	0.05	0.05	0.04
La	1794	1048	1064	561	1831	474	932	956	728		620	85	4.0	3.4	70	57	47	270	143
Ce	2979	1654	1694	1136	4534	1791	3717	3052	2678		2391	274	11	10	162	112	82	454	225
Pr	308	176	168	113	530	279	554	394	428		394	39	3.0	1.7	15	13	8.0	36	17
Nd	1042	562	497	367	1889	1130	2365	1343	1788		1661	223	29	14	54	57	32	125	62
Sm	126	90	84	86	245	187	391	175	302		269	81	30	15	8.4	15	6.7	21	14
Eu	30	22	22	27	56	44	105	42	73		61	23	16	8.0	2.5	4.1	1.6	4.7	4.2
Gd	82	63	65	70	135	91	184	59	153		122	64	52	29	7.7	15	5.1	14	14
Tb	7.6	6.1	6.8	8.8	14	10	21	6.2	16		13	6.8	6.6	3.8	0.68	1.5	0.60	1.4	2.3
Dy	30	25	30	40	56	36	78	23	62		47	27	26	15	2.7	6.6	2.8	6.2	11.5
Ho	4.4	3.7	4.9	6.1	7.8	4.3	9.2	2.4	7.4		5.5	3.8	3.5	2.0	0.44	1.1	0.51	1.0	1.9
Er	7.4	6.6	9.8	11	13	6.3	15	4.1	11		8.0	5.8	5.0	2.7	0.71	1.9	1.0	1.9	3.3
Tm	0.74	0.68	1.1	1.1	1.3	0.58	1.3	0.41	0.96		0.71	0.52	0.32	0.15	0.04	0.17	0.13	0.22	0.34
Yb	3.7	3.5	6.5	5.7	6.5	2.9	5.4	2.2	4.3		3.1	2.0	0.94	0.40	0.13	0.75	0.75	1.2	1.6
Lu	0.43	0.43	0.75	0.49	0.62	0.27	0.38	0.20	0.32		0.24	0.21	0.07	0.03	0.01	0.13	0.11	0.14	0.19
Y	97	85	134	109	108	49	137	37	85		62	63	72	43	13	25	9.5	18	29

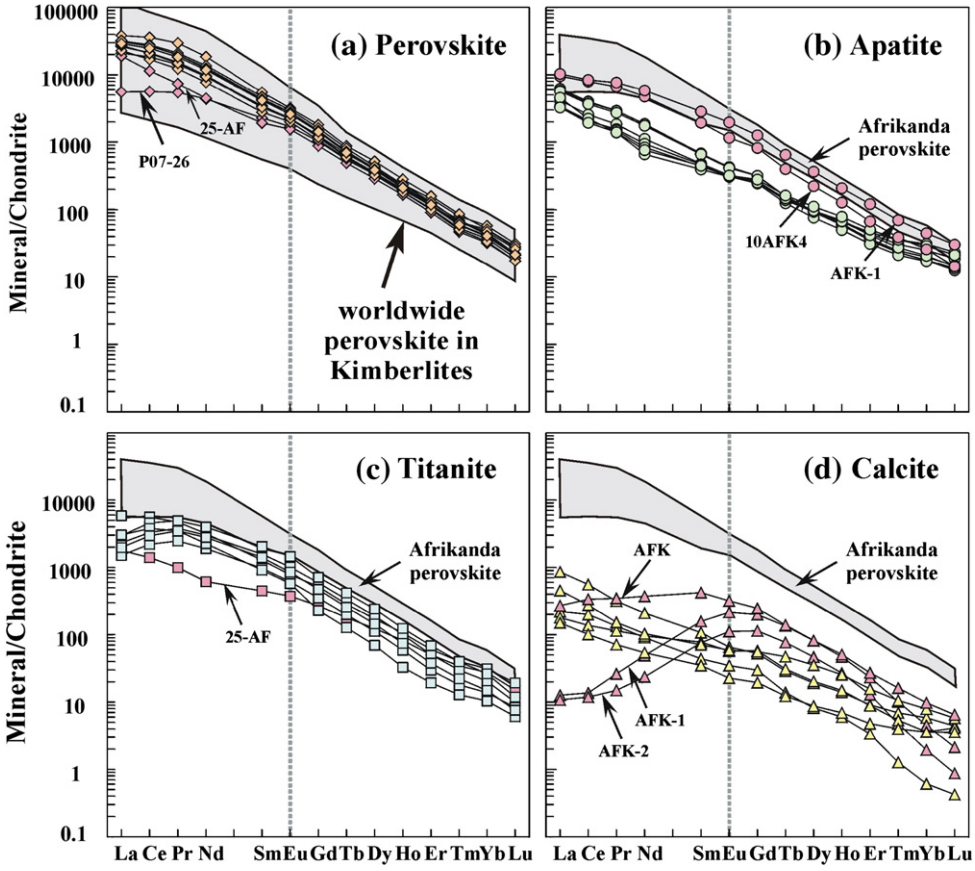

Fig. 5. Rare earth elements (REEs) distribution patterns of perovskite (a), apatite (b), titanite (c) and calcite (d).
Data for kimberlite perovskites were from Chalapathi Rao et al. (2013-this volume), Wu et al. (2010a, 2013-this volume) and Yang et al. (2009).

(0.4–0.9 wt.%). With respect to trace elements, the perovskites are characterized by high concentrations of Sr (2184–3569 ppm), Nb (5115–13,240 ppm), Ta (147–390 ppm), but low Zr (139–390 ppm) and Hf (3.4–8.9 ppm), and minor Rb (0.1–0.7 ppm). The REE distribution patterns show extreme light REE (LREE) enrichment with La abundances of about 19,000–38,000 times higher than those of chondrites and with $(La/Yb)_N$ ratios of 363–811, except sample P07-26 (Fig. 5a).

Apatite occurs in all phases of the complex, but does not show any significant differences. The apatite contains 53.0–54.8 wt.% CaO and 40.4–42.0 wt.% P_2O_5 with minor SiO_2 (0.1–0.8 wt.%) (Table 3). Compared to perovskite, apatite has higher Sr concentrations of 4177–7107 ppm, but lower REE, particularly middle REE, concentrations (Fig. 5b).

Titanite occurs in most phases of the complex. In common with apatite, titanite does not show any compositional differences between these different phases. Most titanites contain ~31 wt.% SiO_2, 31.8–38.6 wt.% TiO_2, and 27.5–28.8 wt.% CaO with minor Al_2O_3 (0.2–3.8 wt.%) and Fe_2O_3 (1.0–2.5 wt.%). With respect to trace elements, titanite has high Nb (1309–6156 ppm), Ta (61–309 ppm), Zr (151–2906 ppm) and Sr (321–779) with low Rb (<0.4 ppm). Titanite has low concentrations of REE with depletions of La and Ce, compared with apatite (Fig. 5c). However, titanite from sample 25-AF has slightly lower LREE contents than those in the other samples (Fig. 5c).

Calcite, as an interstitial mineral, occurs primarily in the 4th phase of the complex (Fig. 4f). As shown in Fig. 5d, calcite from different samples shows variable REE distribution patterns. Most calcite samples are characterized by a steep REE distribution pattern with high light REE and low heavy REE abundances. Calcite from perovskite ore (AFK, AFK-1 and AFK-2) is strongly depleted in LREE and has convex-upward REE distribution patterns (Fig. 5d). It is not clear why this calcite is depleted in LREE although this might result from post-magmatic hydrothermal processes as discussed by Chakhmouradian and Zaitsev (2004).

4.2. Perovskite U–Pb age

Twelve samples of perovskite were extracted from our suite of samples, but only six were selected for U–Pb age determination. For the main (2nd) phase of pyroxenite, perovskite with a grain-size of ~200 μm is associated primarily with apatite (Fig. 3a). Laser ablation analyses of the perovskite from medium-grained pyroxenite of 25-AF yield a $^{206}Pb/^{238}U$ weighted average age of 377 ± 6 Ma with a lower intercept age of 390 ± 9 Ma (Fig. 6a). Perovskite from the 3rd phase pegmatitic perovskite orebody is euhedral and greater than 100 μm in size (Fig. 3b). Centimeter-sized perovskite is interstitially filled by ilmenite (Fig. 3d). With the exception of the in-house standard AFK described above, four samples of euhedral perovskite give $^{206}Pb/^{238}U$ weighted average ages of 385 ± 5 (AFK-1, Fig. 6b), 379 ± 5 (AFK-2, Fig. 6c), 379 ± 4 (AFK-5, Fig. 6d), and 379 ± 5 (10AFK2, Fig. 6e), respectively, and are thus identical within error. Perovskite from the ijolite–melteigite (4th phase) istypically euhedral with grain-sizes ranging from 50 to 300 μm (Fig. 3e and 3f). For sample P07-21, twenty analyses from different grains by laser ablation yielded a lower intercept age of 378 ± 9 Ma with a $^{206}Pb/^{238}U$ weighted average age of 376 ± 5 Ma (Fig. 6f), identical to those obtained from the pyroxenite and pegmatitic perovskite ores.

One previously studied zirconolite-bearing sample (Afrk-1, Wu et al., 2010c) was also selected for baddeleyite U–Pb isotopic analysis.

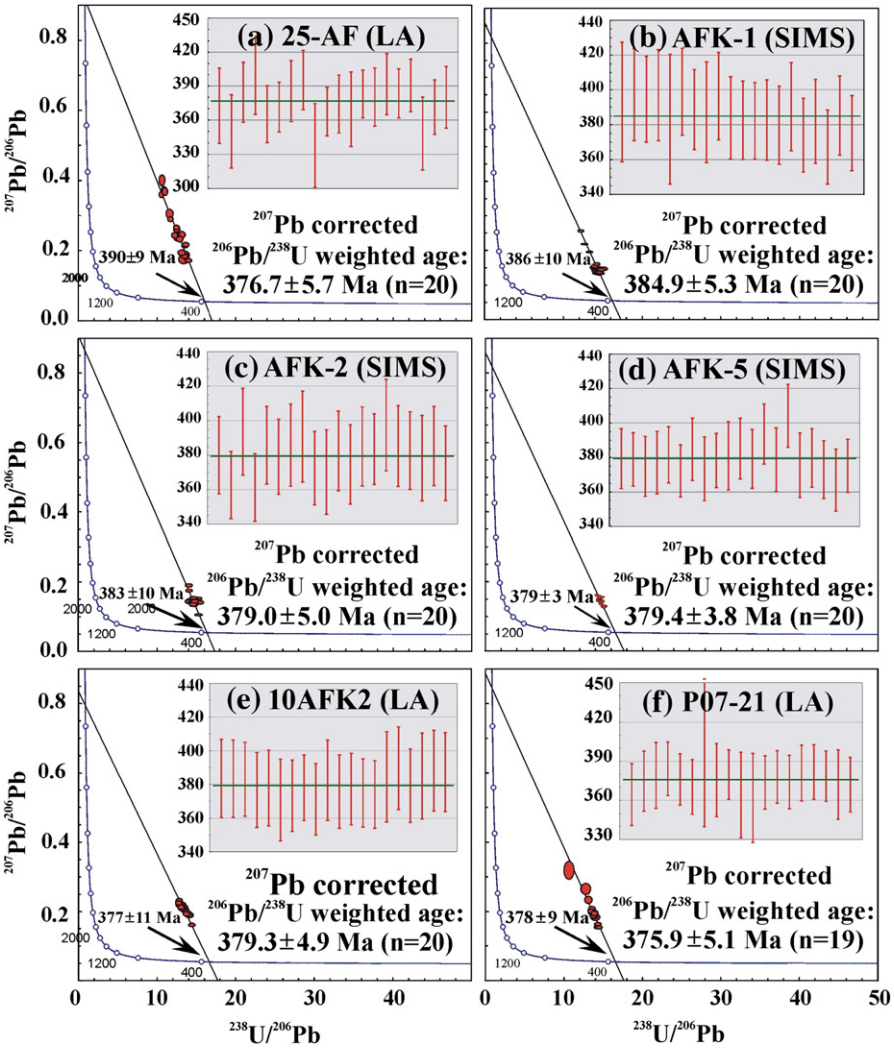

Fig. 6. Terra–Wasserburg U–Pb diagrams of perovskites.

The $^{206}Pb/^{238}U$ age is 374 ± 5 Ma (Fig. 7a), which is identical to the perovskite ages within the analytical errors.

Perovskite from the Arkhangelsk kimberlite (Z1-3-2) was also selected for U–Pb age determination by SIMS techniques. Fourteen analyses yielded the same lower intercept and ^{207}Pb corrected ages of 381 ± 3 Ma (Fig. 7b), identical to those obtained for perovskite from the Afrikanda complex.

4.3. Sr–Nd isotopic compositions

4.3.1. Perovskite

Twelve samples of perovskite were analyzed for their Rb–Sr and Sm–Nd isotopic compositions (Table 4). All of these samples have low $^{87}Rb/^{86}Sr$ ratios (0.00003–0.00018) with $^{87}Sr/^{86}Sr$ ratios ranging from 0.70332 ± 4 to 0.70363 ± 6 (Table 4, Fig. 8a). The $^{147}Sm/^{144}Nd$ and $^{143}Nd/^{144}Nd$ isotopic compositions range from 0.0674 to 0.1053, and from 0.512540 ± 24 to 0.512626 ± 10, respectively (Table 4, Fig. 9a). Perovskite from samples 25-AF and P07-26 is significantly higher in its $^{147}Sm/^{144}Nd$ ratios than the other samples (Fig. 9a).

For the individual phases of the complex (Table 4), the Sr isotopic ratios for the main pyroxenite are 0.70345 ± 5 for sample 25-AF and 0.70359 ± 3 for sample 10AFK3. Their average $^{147}Sm/^{144}Nd$ and $^{143}Nd/^{144}Nd$ ratios are: 0.0904 and 0.512540 ± 24 (25-AF) and 0.0709 and 0.512575 ± 12 (10AFK3), respectively, with $\varepsilon_{Nd}(t)_{380}$ values of +3.3 ± 0.5 and +4.9 ± 0.2 (Table 4). For the perovskite ore, analyses of eight perovskites yielded uniform Sr isotopic ratios ranging from 0.70332 ± 4 (10AFK1) to 0.70340 ± 4 (AFK-2), with $^{87}Rb/^{86}Sr$ ratios from 0.00003 to 0.00018. Their $^{147}Sm/^{144}Nd$ and $^{143}Nd/^{144}Nd$ ratios range from 0.0674 to 0.0758 and from 0.512600 ± 9 to 0.512626 ± 10, respectively, with $\varepsilon_{Nd}(t)_{380}$ values from +5.4 ± 0.2 (AFK-5) to +5.8 ± 0.2 (AFK-2). Perovskite from ijolite–melteigite samples P07-21 and P07-26 gave Sr isotopic ratios of 0.70352 ± 3 and 0.70363 ± 6, respectively. Their $^{147}Sm/^{144}Nd$ and $^{143}Nd/^{144}Nd$ ratios are 0.0753 and 0.1053, and 0.512557 ± 24 and 0.512609 ± 20, respectively, with $\varepsilon_{Nd}(t)_{380}$ values of +4.3 ± 0.5 (P07-21) and +3.9 ± 0.4 (P07-26).

4.3.2. Apatite

Ten apatite samples were selected for Sr–Nd isotopic analysis (Table 4). All have uniform $^{87}Rb/^{86}Sr$ ratios of less than 0.00006 with $^{87}Sr/^{86}Sr$ ratios ranging from 0.70327 ± 5 (10AFK4) to 0.70363 ± 4 (P07-26) (Table 4, Fig. 8b). The exception is sample 25-AF, which has a slightly higher $^{87}Sr/^{86}Sr$ ratio of 0.70412 ± 3, although its $^{87}Rb/^{86}Sr$ ratio of 0.00005 is not unusual, compared with the other samples (Fig. 8b). In terms of Nd isotopic data (Fig. 9b), apatite shows much more variation than perovskite, with $^{147}Sm/^{144}Nd$, $^{143}Nd/^{144}Nd$ and $\varepsilon_{Nd}(t)_{380}$ values ranging from 0.0619 to 0.0944, 0.512430 ± 35 to

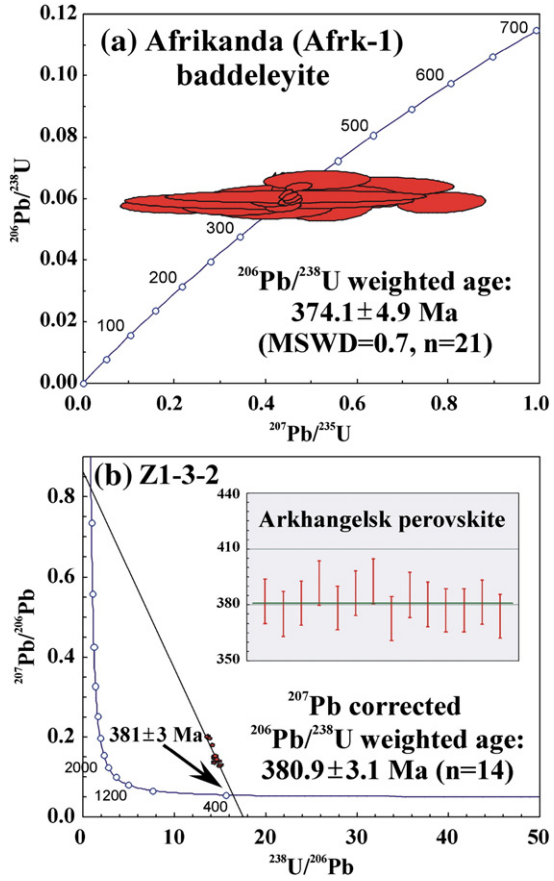

Fig. 7. U–Pb Concordia diagram of the Afrikanda baddeleyite (a) and Terra–Wasserburg diagram of the Arkhangelsk perovskite (b).

0.512674±21 and +1.2±0.7 (25-AF) to +5.7±0.4 (AFK-1), respectively. It is also noted that apatite from samples P07-26 and 25-AF has low Nd contents and is unsuitable for the precise determination of its Nd isotopic composition. However, 25-AF yielded an $^{143}Nd/^{144}Nd$ ratio of 0.512430±35 with a $^{147}Sm/^{144}Nd$ ratio of 0.0894.

4.3.3. Titanite

Titanite was extracted only from eight samples, and has higher $^{87}Rb/^{86}Sr$ ratios (0.0001–0.0029) than perovskite and apatite, with $^{87}Sr/^{86}Sr$ ratios ranging from 0.70336±9 (AFK-1) to 0.70379±18 (10AFK3). Their $^{147}Sm/^{144}Nd$ and $^{143}Nd/^{144}Nd$ isotopic ratios range from 0.0780 to 0.1116, and 0.512585±14 to 0.512714±15, respectively, with $\varepsilon_{Nd}(t)_{380}$ values from +4.2±0.9 (P07-26) to +5.8±0.3 (10AFK5). However, in common with apatite, titanite from sample 25-AF has a high $^{87}Sr/^{86}Sr$ ratio of 0.70425±12 (Fig. 8c). Because of the low Nd content (367 ppm), this sample gives a low and imprecise $^{143}Nd/^{144}Nd$ ratio of 0.512559±86 (Table 4). Similarly, sample P07-25 gives an $^{143}Nd/^{144}Nd$ ratio of 0.512641±46. Excluding these samples, there is no significant Sr and Nd isotopic variation among the titanite from the different petrogenetic phases (Fig. 8c).

4.3.4. Calcite

Calcite has low REE concentrations, thus only Sr isotopic compositions were determined (Table 4). Of the seven samples of calcite extracted from the perovskite ore, AFK has a variable Sr isotopic composition (Fig. 8d), indicating an open Sr isotopic system for this sample. The other calcite samples have uniform $^{87}Rb/^{86}Sr$ (<0.00013) and $^{87}Sr/^{86}Sr$ (from 0.70330±3 for AFK-2 to 0.70342±6 for AFK-5) ratios, comparable to perovskite, apatite and titanite from the same rock type.

5. Discussion

5.1. Emplacement age of the Afrikanda complex

Whole-rock Rb–Sr analyses for a clinopyroxenite yielded an age of 364±3 Ma (Kramm et al., 1993), this being previously considered as the emplacement time of the complex. Recently, Reguir et al. (2010) obtained U–Pb ages of 374±10 and 371±8 Ma for perovskite extracted from pyroxenite and carbonatite, respectively. Initial Sr isotopic ratios reported by them are 0.70333±3 for pyroxenite and 0.70337±2 for carbonatite. Recently, Wu et al. (2010c) obtained $^{207}Pb/^{206}Pb$ ages of 382±12 and 379±6 Ma for calzirtite and zirconolite from a pyroxenite (Afrk-1) and 382±7 Ma for zirconolite from another pyroxenite (Afrk-2) (Table 5), suggesting that the Afrikanda complex might be older than previously thought.

In this study, numerous U–Pb age determinations of perovskite have been undertaken. Perovskite from pyroxenite (25-AF, 2nd phase of the complex) gives an age of 377±6 Ma (Fig. 6a). Apart from the previously described AFK sample (which has a TIMS U–Pb age of 382±1 (Fig. 4) and a SIMS U–Pb age of 383±4 Ma), four other samples of perovskite (AFK-1, AFK-2, AFK-5 and 10AFK2) from the perovskite orebody gave U–Pb ages ranging from 379±5 to 385±5 Ma (Fig. 6b–e), identical to those of the perovskite AFK. U–Pb isotopic analyses of the baddeleyite associated with zirconolite yield an age of 374±5 Ma (Fig. 7a). Perovskite from the melteigite (P07-21, 3rd phase of the intrusion) yielded a $^{206}Pb/^{238}U$ age of 376±5 Ma (Fig. 6f). The weighted average age of these data is 381.3±1.7 Ma (n=9) (Fig. 10). These ages are consistent with those previously obtained from zirconolite and calzirtite by Wu et al. (2010c). Therefore, it is concluded that the Afrikanda complex was emplaced at ~380 Ma.

However, not all of the ages of the complexes in the KAP have been well-constrained (Downes et al., 2005). Using the TIMS method, Amelin and Zaitsev (2002) determined that the Kovdor complex in the area was emplaced at ~378 Ma, an age which was verified by Bayanova (2006) and Wu et al. (2010c). Recently, Rodionov et al. (2012) obtained a concordant age of 379±4 Ma for carbonatite and phoscorite. To check the reliability of these ages, we analyzed perovskite and baddeleyite from a Kovdor pyroxenite using the SIMS method described here and determined ages of 382±3 (perovskite) and 374±5 (baddeleyite) Ma (Table 5). Therefore, it can be concluded that the Kovdor complex was emplaced at ~378 Ma (Fig. 10).

For other alkaline ultramafic complexes in the Kola Peninsula, reliable U–Pb ages are: 378±4 Ma (Seblyavr, U–Pb baddeleyite, Bayanova, 2006); 382±5 Ma (Seblyavr, Th–Pb calcite, dolomite and whole-rock, Rukhlov and Bell, 2010); 377±4 Ma (Vuorijarvi, U–Pb baddeleyite, Bayanova, 2006); 387±7 Ma (Kurga, U–Pb zircon, Bayanova, 2006); 372±3 Ma (Sallanlatva, U–Pb zircon, Zaitsev et al., 2004); 374±8 Ma (Lesnaya Varaka, U–Pb perovskite, Matukov et al., 2006); 380±7 Ma (Sokli, U–Pb apatite, Rukhlov and Bell, 2010); 386±3 Ma (Kandaguba, Th–Pb apatite, Rukhlov and Bell, 2010). For the Turiy complex, the ages include 377±4 Ma (U–Pb zircon, phoscorite), 376±6 Ma (U–Pb baddeleyite, carbonatite), and 383±2 Ma (U–Pb garnet and titanite, nephelinite) (Rukhlov and Bell, 2010). Zircons from the Kandalaksha carbonatite also give the similar ages (380±7 and 378±8 Ma, Claesson et al., 2000). These ages yield a weighted value of 380.9±2.3 (n=13) (Fig. 10), indicating that the alkaline ultramafic and carbonatitic complexes of the KAP were emplaced at about 380 Ma, and are contemporaneous with the Afrikanda complex.

The age of the "kimberlitic" rocks in the area is not well known. According to the available data, "kimberlite" is found mostly in the Arkhangelsk area (SE of the area, Fig. 1), and is considered by Downes

Table 4
Sr–Nd isotopic data of the Afrikanda complex.

Sample	Phase	Rock type	Mineral	$^{87}Rb/^{86}Sr$	$^{87}Sr/^{86}Sr$	2σ	$^{147}Sm/^{144}Nd$	$^{143}Nd/^{144}Nd$	2σ	T_{DM}	$\varepsilon_{Nd}(t)$	2σ	$f_{Sm/Nd}$
25-AF	2nd	Pyroxenite	Prv	0.00003	0.70345	5	0.0904	0.512540	24	755	3.25	0.47	−0.54
25-AF	2nd	Pyroxenite	Ap	0.00005	0.70412	3	0.0894	0.512430	35	883	1.15	0.68	−0.55
25-AF	2nd	Pyroxenite	Tit	0.00034	0.70425	12	0.1185	0.512559	86	946	2.26	1.68	−0.40
10AFK3	2nd	Pyroxenite	Prv	0.00003	0.70359	3	0.0709	0.512575	12	615	4.88	0.23	−0.64
10AFK3	2nd	Pyroxenite	Ap	0.00001	0.70357	2	0.0909	0.512477	32	835	2.00	0.62	−0.54
10AFK3	2nd	Pyroxenite	Tit	0.00011	0.70379	18	0.0780	0.512585	14	635	4.73	0.27	−0.60
AFK(TIMS)	3rd	Perovskite ore	Prv	0.00141	0.70335	3	0.0659	0.512604	14	564	5.69	0.27	−0.66
AFK	3rd	Perovskite ore	Prv	0.00008	0.70335	4	0.0680	0.512612	6	564	5.75	0.12	−0.65
AFK	3rd	Perovskite ore	Tit	0.00007	0.70341	5	0.1069	0.512675	20	679	5.09	0.39	−0.46
AFK	3rd	Perovskite ore	Cc	0.00002	0.70447	56							
AFK-1	3rd	Perovskite ore	Prv	0.00009	0.70336	5	0.0707	0.512609	10	577	5.56	0.20	−0.64
AFK-1	3rd	Perovskite ore	Ap	0.00006	0.70328	4	0.0944	0.512674	21	609	5.67	0.41	−0.52
AFK-1	3rd	Perovskite ore	Tit	0.00031	0.70336	9	0.1012	0.512673	9	647	5.32	0.18	−0.49
AFK-1	3rd	Perovskite ore	Cc	0.00000	0.70333	3							
AFK-2	3rd	Perovskite ore	Prv	0.00009	0.70340	4	0.0674	0.512615	12	558	5.83	0.23	−0.66
AFK-2	3rd	Perovskite ore	Tit	0.00294	0.70369	9	0.0831	0.512601	9	641	4.80	0.18	−0.58
AFK-2	3rd	Perovskite ore	Cc	0.00001	0.70330	3							
AFK-5	3rd	Perovskite ore	Prv	0.00008	0.70337	4	0.0711	0.512600	9	588	5.36	0.18	−0.64
AFK-5	3rd	Perovskite ore	Cc	0.00013	0.70342	6							
10AFK1	3rd	Perovskite ore	Prv	0.00003	0.70332	4	0.0758	0.512626	10	580	5.64	0.20	−0.61
10AFK1	3rd	Perovskite ore	Cc	0.00001	0.70334	7							
10AFK2	3rd	Perovskite ore	Prv	0.00003	0.70339	4	0.0740	0.512612	10	588	5.45	0.20	−0.62
10AFK2	3rd	Perovskite ore	Cc	0.00000	0.70336	11							
10AFK4	3rd	Perovskite ore	Prv	0.00003	0.70336	4	0.0762	0.512613	10	596	5.37	0.20	−0.61
10AFK4	3rd	Perovskite ore	Ap	0.00001	0.70327	5	0.0754	0.512621	26	584	5.56	0.51	−0.62
10AFK4	3rd	Perovskite ore	Tit	0.00010	0.70344	7	0.1052	0.512698	18	636	5.62	0.35	−0.47
10AFK4	3rd	Perovskite ore	Cc	0.00000	0.70330	3							
10AFK5	3rd	Perovskite ore	Prv	0.00005	0.70339	5	0.0703	0.512609	14	576	5.57	0.27	−0.64
10AFK5	3rd	Perovskite ore	Tit	0.00013	0.70339	4	0.1080	0.512714	15	629	5.79	0.29	−0.45
10AFK5	3rd	Perovskite ore	Cc	0.00000	0.70336	6							
P07-21	4th	Melteigite	Prv	0.00008	0.70352	3	0.0753	0.512557	24	654	4.32	0.47	−0.62
P07-21	4th	Melteigite	Ap	0.00001	0.70355	3	0.0805	0.512466	39	783	2.29	0.76	−0.59
P07-22	4th	Melteigite	Ap	0.00001	0.70347	3	0.0707	0.512544	32	647	4.29	0.62	−0.64
P07-23	4th	Ijolite	Ap	0.00000	0.70351	3	0.0619	0.512501	28	652	3.87	0.55	−0.69
P07-24	4th	Ijolite	Ap	0.00001	0.70340	3	0.0701	0.512480	26	712	3.07	0.51	−0.64
P07-25	4th	Melteigite	Ap	0.00003	0.70348	3	0.0761	0.512443	23	784	2.05	0.45	−0.61
P07-26	4th	Melteigite	Prv	0.00018	0.70363	6	0.1053	0.512609	20	761	3.87	0.39	−0.46
P07-26	4th	Melteigite	Ap	0.00003	0.70363	4							
P07-26	4th	Melteigite	Tit	0.00240	0.70371	12	0.1116	0.512641	46	760	4.19	0.90	−0.43
Z1-3-2	Arkhangelsk	Kimberlite	Prv	0.00010	0.70349	15	0.0744	0.512624	12	576	5.67	0.23	−0.62
Afrk-1[a]	3rd	Pyroxenite	Clz				0.1810	0.512870	20		5.54	0.28	−0.08
Afrk-1[a]	3rd	Pyroxenite	Zrn				0.1457	0.512830	11		6.18	0.19	−0.26
Afrk-1[a]	3rd	Pyroxenite	Cc	0.00009	0.70331	3							
Afrk-2[a]	3rd	Pyroxenite	Zrn				0.1435	0.512823	10		6.21	0.19	−0.27
Afrk-2[a]	3rd	Pyroxenite	Cc	0.00027	0.70319	4							

[a] Data from Wu et al. (2010c).

et al. (2005) to be a part of the Devonian alkaline magmatism in the Kola Peninsula. Perovskite extracted from Arkhangelsk kimberlite (Z1-3-2 of Beard et al., 2000) gave a U–Pb age of 381 ± 3 (Fig. 7b), which is identical to those of alkaline ultramafic and carbonatitic rocks. It is also interesting to note that this perovskite has similar Sr and Nd isotopic compositions to other rocks within the KAP (Table 4), but distinctly different from the whole-rock data by Beard et al. (2000).

The KAP is also characterized by the large agpaitic Khibiny and Lovozero complexes. The lack of suitable minerals in these complexes limits their precise age determination. Eleven Rb–Sr isochron ages for the syenite and pyroxenite xenoliths from the Khibiny complex range from 358 to 377 Ma (Kramm et al., 1993; Kramm and Kogarko, 1994; Arzamastsev and Belyatsky, 2000; Waight et al., 2002; Arzamastsev et al., 2003). The Ar–Ar age from the Khibiny alkaline dyke swarm ranges from 388 ± 6 Ma for hornblende in the alkaline lamprophyre to 363 ± 5 Ma for phlogopite in an alkali picrite which cuts the nepheline syenite (Arzamastsev et al., 2005, 2007). In terms of U–Pb analyses, the ages obtained from four eudialyte syenites vary from 358 to 368 Ma (Wu et al., 2010b). Recently, analyses of loparite yielded a U–Pb age of 374 ± 3 Ma (Mitchell et al., 2011), and are the most precise estimation of the age of this agpaitic complex.

For Lovozero, three Rb–Sr isochrons yielded ages between 362 and 372 Ma (Kramm et al., 1993; Kramm and Kogarko, 1994). The U–Pb age determined by Mitchell et al. (2011) for loparite using a laser ablation technique is 373 ± 2 Ma, identical to the TIMS age (376 ± 1 Ma) given by Oversby and Ringwood (1981). The zircon U–Pb ages determined by Arzamastsev et al. (2007) are much younger (347 to 359 Ma) than those of the loparite. These zircons, with high Th/U ratios, are from a microcline-albite pegmatite, and represent the age of later thermal activity. It was concluded by Mitchell et al. (2011) that the Lovozero and Khibiny complexes are coeval and emplaced at ~375 Ma.

It has been argued that the Paleozoic alkaline magmatism in the KAP might be initiated much earlier than 400 Ma. However, these older ages were mostly obtained by Rb–Sr isochron techniques, and are undoubtedly not reliable. For example, the Rb–Sr isochron ages of the Kurga and Seblyavr complexes are 404 ± 10 and 404 ± 10 Ma, whereas their zircon and baddeleyite U–Pb ages are 387 ± 7 and 378 ± 4 Ma, respectively (Bayanova et al., 1998). Therefore, we

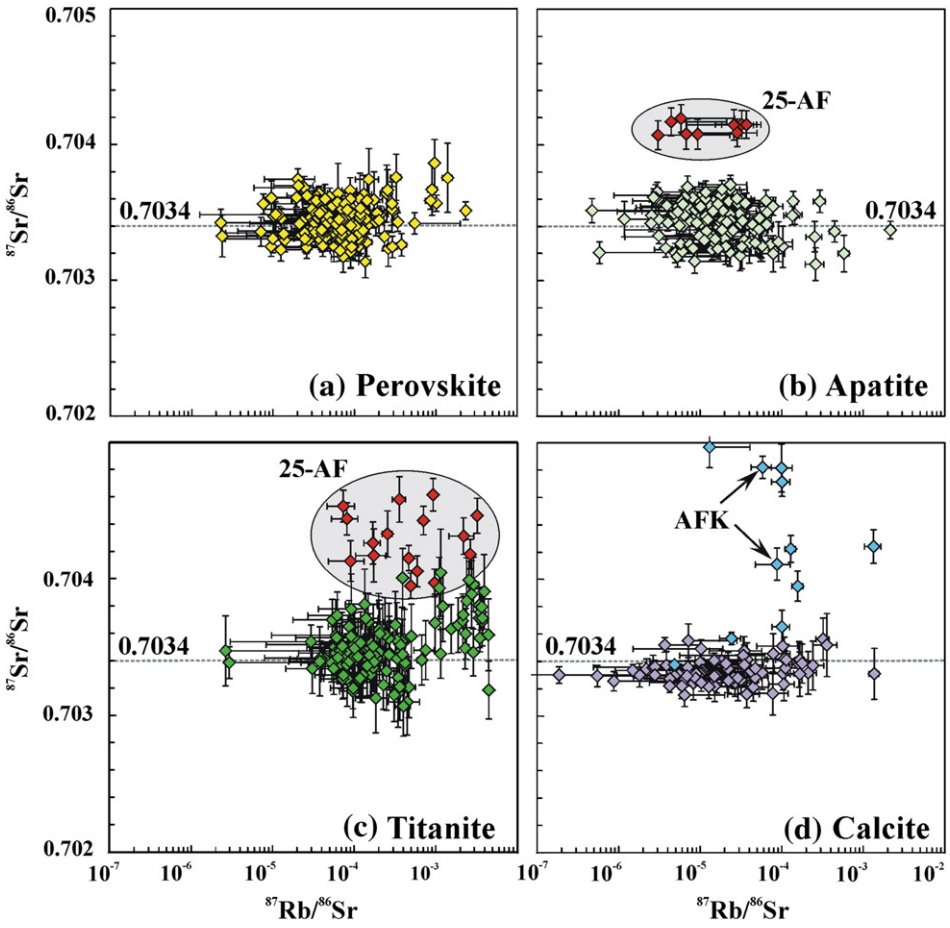

Fig. 8. In situ Sr isotopic variations of perovskite (a), apatite (b), titanite (c) and calcite (d).

conclude (Table 5, Fig. 10), that the alkaline ultramafic (Afrikanda, Kovdor, etc.) and "kimberlitic" magmatism in the KAP occurred contemporaneously at ~380 Ma, and that the agpaitic syenites (Khibiny and Lovozero) was emplaced at ~375 Ma, indicating that these complexes are slightly younger than the alkaline ultramafic, carbonatitic and "kimberlitic" rocks. More data are required to verify this conclusion. An alternative explanation of these data is that the Kola alkaline magmatism occurred continuously from 375 to 380 Ma with a duration of ~5–10 Ma.

5.2. Isotopic constraints on the petrogenesis of the Afrikanda complex

The Afrikanda complex consists mainly of dunite (10 vol.%), pyroxenite (70 vol.%) and ijolite–melteigite (20 vol.%) with minor carbonatite (Arzamastsev and Mitrofanov, 2009). The question of how these rocks are genetically related remains unanswered, i.e., whether they are products of fractional crystallization of a common magma or products of crystallization from independent mantle-derived magmas. Chakhmouradian and Zaitsev (2004) suggested that the Afrikanda carbonatite crystallized from a carbonatitic magma derived from a carbonate amphibole wehrlite; whereas the silicate rocks (pyroxenite and ijolite–melteigite) crystallized from a melanephelinitic magma which was derived by partial-melting of an amphbole- and phlogopite-bearing lherzolite. These authors suggested that the silicate and carbonatitic rocks within the complex have different magmatic sources and could not be derived from the same parental magma by crystal fractionation.

There is no evidence to suggest that the Afrikanda complex was formed by liquid immiscibility, as advocated by Chakhmouradian and Zaitsev (2004). Thus textures indicative of liquid immiscibility are not observed. Such textures, with globules of carbonate-rich material within a silicate matrix (or silicate-rich material within a carbonate matrix), are critical for identifying the liquid immiscibility. Further, the pyroxenites exhibit typical cumulate textures, indicating crystal fractionation during magma crystallization. Finally, the complex, except for the melteigite–ijolite, changes rock types gradationally from an outer nepheline-bearing pyroxenite to an inner medium-to-coarse grained pyroxenite. In addition, geochemical data for the major elements indicate that Afrikanda rocks do not conform to the model of liquid immiscibility predicted by Lee and Wyllie (1998) (Chakhmouradian and Zaitsev, 2004).

It was determined in this study that each intrusive phase shows some Sr–Nd isotopic variations (Fig. 11). For the main phase of medium- to coarse-grained pyroxenite, samples 25-AF and 10AFK3 show variable Sr and Nd isotopic compositions (Fig. 11a). These samples also show inter-mineral variations in terms of Sr and Nd isotopic compositions (Fig. 11a), which are considered to result from crustal contamination during crystallization. Supporting evidence is provided by sample 25-AF which is located not far from the contact zone between the complex and the surrounding gneiss. Alternatively, these samples could have been reset with respect to their Sr and Nd isotopic systematics during later thermal activity. For example, petrographic examination shows that perovskite in sample 25-AF is mostly replaced by titanite, indicating sub-solidus reaction during thermal overprinting. Considering

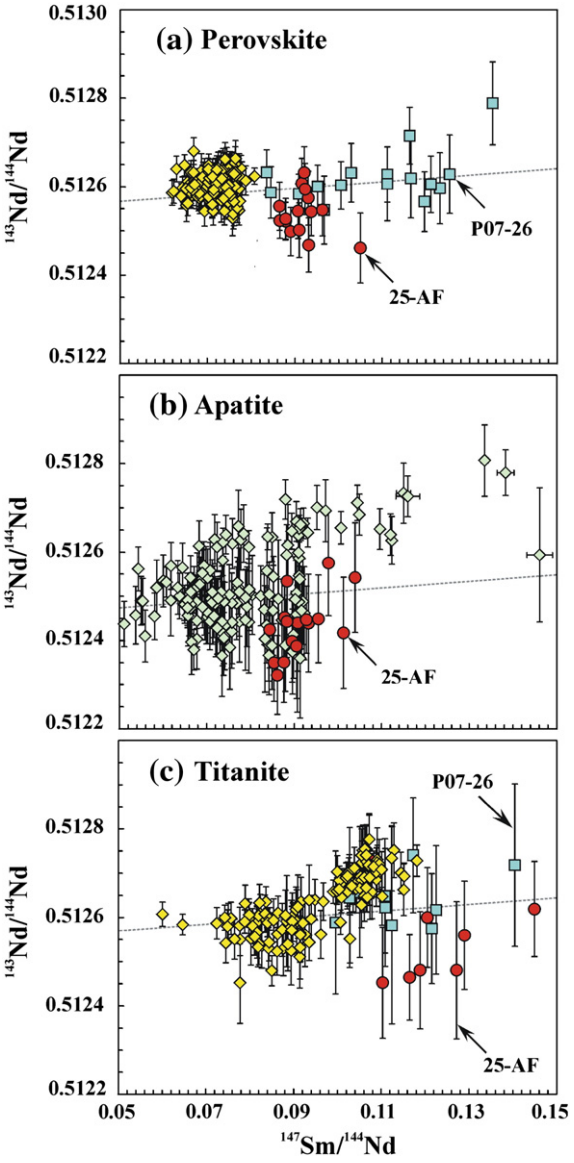

Fig. 9. In situ Nd isotopic variations of perovskite (a), apatite (b) and titanite (c).

that perovskite can better preserve its Sr and Nd isotopic systematics compared to apatite and titanite, and thus it records the primary isotopic compositions of magma. The pegmatitic perovskite ore from the 3rd phase of the complex, has the most primitive Sr and Nd isotopic compositions (Fig. 11b). In addition, perovskite, titanite and calcite from these calcite-bearing perovskite ore samples have uniform Sr and Nd isotopic compositions (Table 4 and Fig. 11b), which is thought to represent the primary isotopic character of the carbonatitic magma as these perovskite ore samples contain as much as 90 vol.% of calcite sometimes according to our field investigation. The exception is that titanite from AFK-2 has a slight Sr and Nd isotopic deviation from perovskite (Fig. 11a). The ijolite–melteigite of the 4th phase of intrusions have slightly higher Sr and lower $\varepsilon_{Nd}(t)$ value than the perovskite orebodies (Fig. 11c), but comparable to those of perovskite obtained from the 2nd phase of pyroxenite. Therefore, the silicate (2nd and 4th phases) and carbonatitic (3rd phase) rocks within the complex are not co-genetic by either crystal fractionation or liquid immiscibility from a common magma, as have been previously proposed by Chakhmouradian and Zaitsev (2004). The silicate magma has an $^{87}Sr/^{86}Sr$ ratio of ~0.7034 to ~0.7038 and a positive $\varepsilon_{Nd}(t)_{380}$ value of +2.0 to +4.9, whereas the carbonatitic magma is isotopically more primitive with an $^{87}Sr/^{86}Sr$ ratio of ~0.7033 to ~0.7035 and $\varepsilon_{Nd}(t)_{380}$ value of +5.1 to +5.8 (Fig. 11d). Therefore, the silicate and carbonatitic magmas could be derived from mantle sources with a small degree of isotopic heterogeneity. Alternatively, the parent magma of silicate rocks could be crustally contaminated before its emplacement at the present level.

5.3. Geodynamic setting

Alkaline ultramafic and agpaitic magmatism is widespread during evolution of the Earth, especially within the stable cratons. However, the geodynamic factors controlling the origin of this kind of rock remain unclear. According to this study, the Kola Peninsula is characterized by coeval igneous rocks of alkaline ultramafic, agpaitic, "kimberlitic", carbonatitic, and melilititic affinities during the Devonian. Considering that these intrusions were emplaced within a short duration from 375 to 380 Ma and with a large volume of 15,000–75,000 km^3, it is widely accepted that this alkaline magmatism was related to mantle plume activity (Arzamastsev et al., 2001; Downes et al., 2005; Arzamastsev et al., 2010), a conclusion also supported by noble gas geochemistry (Marty et al., 1998; Tolstikhin et al., 2002).

The Afrikanda complex is isotopically depleted with low initial Sr ($^{87}Sr/^{86}Sr = 0.7033$ to 0.7038) and high initial Nd isotopic compositions ($\varepsilon_{Nd}(t)_{380} = +2.0$ to +5.8). According to the available data, the alkaline ultramafic complexes of Kovdor, Seblyavr, Vuoriyarvi, Kurga and Turiy have low initial $^{87}Sr/^{86}Sr$ ratios and positive $\varepsilon_{Nd}(t)_{380}$ values, as shown in Fig. 11 (Zaitsev and Bell, 1995; Verhulst et al., 2000; Downes et al., 2005; Lee et al., 2006; Balaganskaya et al., 2007; Wu et al., 2010c). For the agpaitic rocks in the area (Fig. 12a), analyses of eudialyte and loparite show that the Khibiny and Lovozero complexes have low initial $^{87}Sr/^{86}Sr$ (0.7034 to 0.7038) and high $\varepsilon_{Nd}(t)_{380}$ (+3.5 to +5.7) values (Wu et al., 2010b; Mitchell et al., 2011). These data are comparable to the previous results obtained from whole-rock samples (Kramm et al., 1993, Kramm and Kogarko, 1994; Zaitsev et al., 2002; Sindern et al., 2004). The Niva agpaitic complex has identical isotopic composition to the Khibiny and Lovozero complexes (Arzamastsev et al., 2000), which indicates derivation from an isotopically depleted mantle source similar to that of the alkaline ultramafic magmas (Fig. 12b). Carbonatites in the area (such as the Khibiny, Kovdor, Seblyavr, Vuoriyarvi, Sokli, Kandalaksha and Turiy complexes) share the same Sr–Nd isotopic compositions as the ultramafic and agpaitic rocks (Fig. 12c, Kramm et al., 1993; Zaitsev and Bell, 1995; Verhulst et al., 2000; Dunworth and Bell, 2001; Zaitsev et al., 2002; Downes et al., 2005; Lee et al., 2006; Balaganskaya et al., 2007). The exception is the "kimberlites" from the Arkhangelsk region. These rocks show mostly high $^{87}Sr/^{86}Sr$ (0.7034 to 0.7083) and negative $\varepsilon_{Nd}(t)_{380}$ (−7.4 to +2.7) values (Fig. 12d, Beard et al., 2000; Mahotkin et al., 2000). However, our data for perovskite from one "kimberlite" (Z1-3-2) yielded similar Sr–Nd isotopic compositions to those of the alkaline ultramafic, agpaitic and carbonatitic rocks (Table 4), and we ascribe the large Sr–Nd isotopic variations of the whole-rock samples to the crustal contamination during magmatic crystallization, and later weathering and alteration after emplacement. Therefore, the alkaline ultramafic, agpaitic, carbonatitic and "kimberlitic" rocks in the area share a similar Sr–Nd isotopic composition. Additionally, numerical modeling indicates that the mantle source of the alkaline complexes is not primitive in terms of trace elements, but is enriched in incompatible elements and contains metasomatic minerals such as phlogopite and/or amphibole (Arzamastsev et al., 2001). Therefore, it is concluded that the mantle source is isotopically depleted, but incompatible element enriched.

However, an unsolved question is whether this metasomatized mantle is genetically related to the common asthenosphere, pre-existing lithosphere and/or plume material (Bell and Rukhlov,

Table 5
U–Pb isotopic ages of alkaline-ultramafic rocks in the Kola Peninsula, Russia.

Sample	Complex	Rock type	Age (Ma)	2σ	Method	Mineral	Reference
	Afrikanda	Pyroxenite	374	10	U–Pb (LA)	Perovskite	Reguir et al. (2010)
	Afrikanda	Carbonatite	371	8	U–Pb (LA)	Perovskite	Reguir et al. (2010)
Afrk-1	Afrikanda	Pyroxenite	382	12	Pb–Pb (SIMS)	Calzirtite	Wu et al. (2010c)
Afrk-1	Afrikanda	Pyroxenite	379	6	Pb–Pb (SIMS)	Zirconolite	Wu et al. (2010c)
Afrk-2	Afrikanda	Pyroxenite	382	7	Pb–Pb (SIMS)	Zirconolite	Wu et al. (2010c)
P07-21	Afrikanda	Melteigite	376	5	U–Pb (LA)	Perovskite	This paper
25-AF	Afrikanda	Pyroxenite	377	6	U–Pb (LA)	Perovskite	This paper
10AFK2	Afrikanda	Perovskite ore	379	5	U–Pb (LA)	Perovskite	This paper
AFK	Afrikanda	Perovskite ore	382	1	U–Pb (TIMS)	Perovskite	This paper
AFK	Afrikanda	Perovskite ore	383	4	U–Pb (SIMS)	Perovskite	This paper
AFK-1	Afrikanda	Perovskite ore	385	5	U–Pb (SIMS)	Perovskite	This paper
AFK-2	Afrikanda	Perovskite ore	379	5	U–Pb (SIMS)	Perovskite	This paper
AFK-5	Afrikanda	Perovskite ore	379	4	U–Pb (SIMS)	Perovskite	This paper
Afrk-1	Afrikanda	Pyroxenite	374	5	U–Pb (SIMS)	Baddeleyite	This paper
	Kovdor	Phoscorite	378.6	0.2	U–Pb (TIMS)	Baddeleyite	Amelin and Zaitsev (2002)
	Kovdor	Carbonatite	377.5	0.9	U–Pb (TIMS)	Zircon	Amelin and Zaitsev (2002)
	Kovdor	Phoscorite	382	3	U–Pb (TIMS)	Baddeleyite	Bayanova (2006)
	Kovdor	Carbonatite/Phoscorite	379	4	U–Pb (SIMS)	Baddeleyite	Rodionov et al. (2012)
	Kovdor	Pyroxenite	380	5	Pb–Pb (SIMS)	Zirconolite	Wu et al. (2010c)
KV-2	Kovdor	Pyroxenite	374	5	U–Pb (SIMS)	Baddeleyite	This paper
KV-2	Kovdor	Pyroxenite	382	3	U–Pb (SIMS)	Perovskite	This paper
	Seblyavr	Carbonatite	378	4	U–Pb (TIMS)	Baddeleyite	Bayanova (2006)
	Seblyavr	Carbonatite	382	5	Th–Pb (TIMS)	Carbonate/WR	Rukhlov and Bell (2010)
	Vuorijarvi	Carbonatite	377	4	U–Pb (TIMS)	Baddeleyite	Bayanlova (2006)
	Kurga	Pyroxenite	387	7	U–Pb (TIMS)	Zircon	Bayanova et al. (1998)
	Sallanlatva	Carbonatite	375	5	U–Pb (LA)	Zircon	Zaitsev et al. (2004)
	Lesnaya Varaka	Pyroxenite	374	8	U–Pb (SIMS)	Perovskite	Matukov et al. (2006)
	Solki		380	7	Th-Pb (TIMS)	Apatite	Rukhlov and Bell (2010)
951-9	Kandaguba		386	3	Th-Pb (TIMS)	Apatite	Rukhlov and Bell (2010)
C-18-30	Turiy	Phoscorite	377	4	U–Pb (TIMS)	Zircon	Rukhlov and Bell (2010)
T-19/115	Turiy	Carbonatite	376	6	U–Pb (TIMS)	Baddeleyite	Rukhlov and Bell (2010)
W-75	Turiy	Carbonatite	383	2	U–Pb (TIMS)	Garnet/titanite	Rukhlov and Bell (2010)
OTK-2	Kandalaksha	Carbonatite	378	8	U–Pb (SIMS)	Zircon	Claesson et al. (2000)
OTK-3	Kandalaksha	Carbonatite	380	7	U–Pb (TIMS)	Zircon	Claesson et al. (2000)
Z1-3-2	Arkhangelsk	Kimberlite	381	3	U–Pb (SIMS)	Perovskite	This paper
	Khibiny	Ne syenite	374	3	U–Pb (LA)	Loparite	Mitchell et al. (2011)
	Lovozero	Ne syenite	376	1	U–Pb (TIMS)	Loparite	Oversby and Ringwood (1981)
	Lovozero	Ne syenite	373	2	U–Pb (LA)	Loparite	Mitchell et al. (2011)

2004; Bell and Simonetti, 2010). Studies of the mantle peridotitic xenoliths from the nearby Finland kimberlites indicate that the lithospheric mantle during the late Neoproterozoic time was refractory and had a Paleoproterozoic–Archean formation age, as constrained by Os isotopes (Peltonen and Brugmann, 2006). This conclusion is supported by the enriched Nd isotopic composition [ε_{Nd}(370 Ma) value is ~−5.3] obtained for mantle peridotite from the Khibiny complex (Arzamastsev and Glaznev, 2008). Therefore,

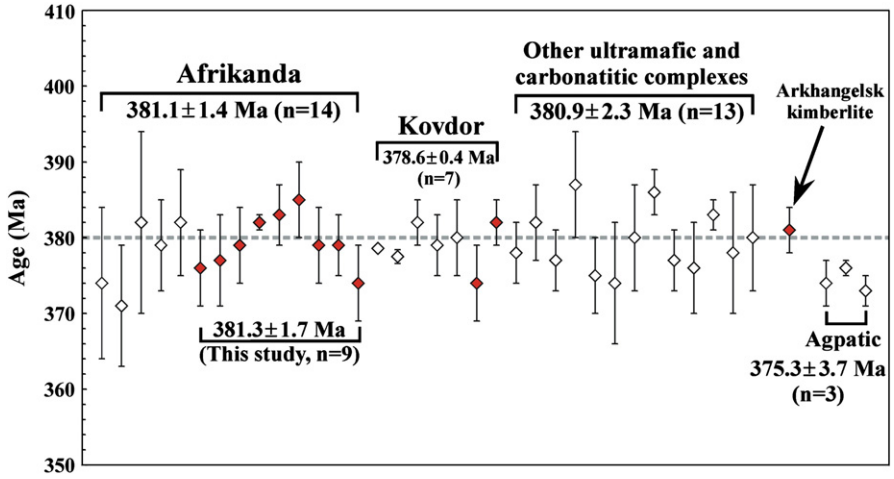

Fig. 10. Age summary of the alkaline ultramafic, agpaitic, carbonatitic and kimberlitic rocks in the KAP. Detailed data can be found in Table 5 with new perovskite U–Pb age determinations shown as red diamonds.

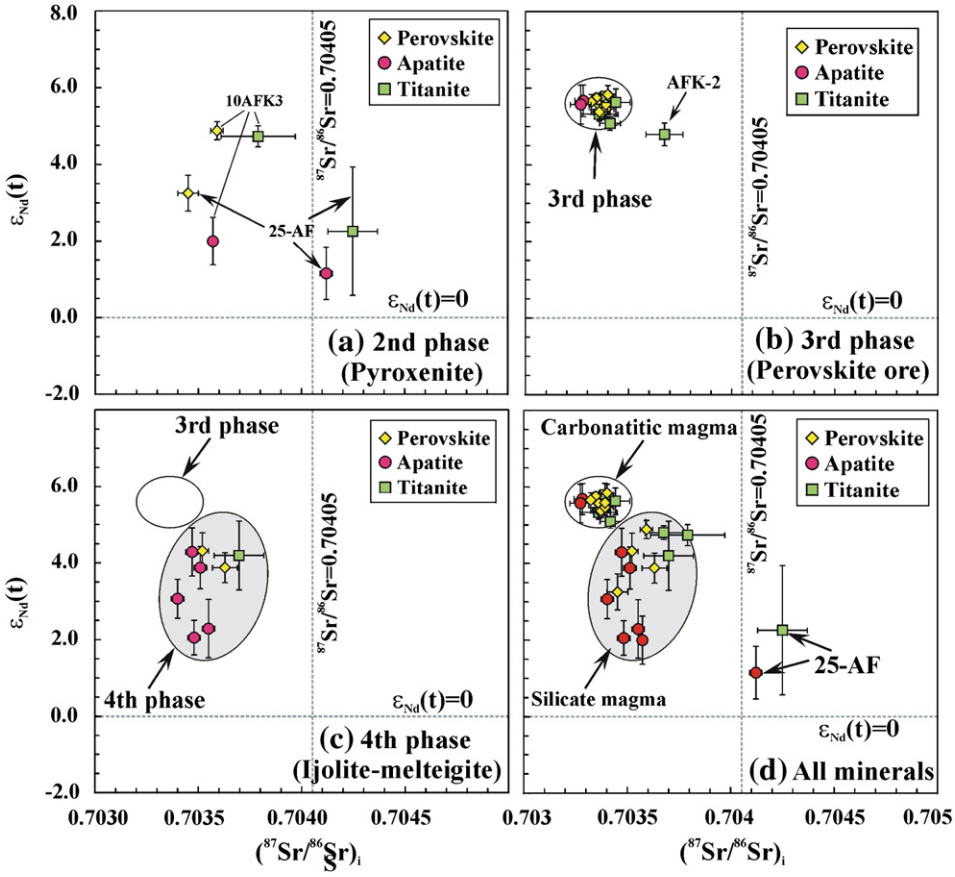

Fig. 11. Sr–Nd isotopic variations of the different phases of the Afrikanda complex.

it is concluded that the ancient sub-KAP lithospheric mantle was not the source of alkaline and carbonatitic magma during the Devonian.

In summary, isotopic data obtained in this study, and other published sources, clearly indicate that the magmas originated from a depleted mantle which is much different from an enriched ancient lithospheric mantle which is high in initial $^{87}Sr/^{86}Sr$ with negative ε_{Nd} values. This depleted mantle could be the convecting mantle beneath the lithosphere, or a deep mantle plume. As suggested by numerous studies (see Bell and Simonetti, 2010), the isotopic composition constrained in the present study is less depleted than the typical end-member of the depleted mantle. Combined with the short duration of magmatic activity, therefore, it is reasonable to accept that the formation of these alkaline rocks is related to mantle plume activity with partial melting during decompression en route to shallow depths. The high alkali contents, high degree of silica-underaturation and strongly fractionated REE distribution patterns of the rocks probably require a small degree of partial melting in deep mantle (Arzamastsev et al., 2001; Downes et al., 2005; Burke et al., 2007).

6. Conclusions

Comprehensive age determinations and Sr–Nd isotopic analyses of perovskite, apatite, titanite and calcite from the Afrikanda complex lead to the following conclusions:

1) Perovskites from pyroxenite, calcite-bearing perovskite ore and ijolite–melteigite yield identical U–Pb ages of 377 ± 6, 379 ± 5–385 ± 5 and 376 ± 5 Ma, respectively with an average value of 381 ± 2 Ma, indicating that the different phases of the complex were contemporaneously emplaced at ~380 Ma;
2) Sr–Nd isotopic analyses of perovskite, apatite, titanite and calcite indicate that the complex was derived from depleted mantle. The silicate and carbonatitic rocks have shown different isotopic compositions, indicating that they might not be cogenetic from a single magma by simple crystal fractionation. However, the silicate rocks could be contaminated with radiogenic Sr and all rocks derived from a single magma or a common source;
3) Perovskite U–Pb ages indicate that the Afrikanda complex was formed contemporaneously with other alkaline ultramafic, carbonatite, "kimberlitic" and agpaitic rocks in the area, their similar Sr–Nd isotopic compositions suggest that the Kola alkaline magmatism was probably controlled by mantle plume activity.

Acknowledgments

Hilary Downes is thanked for kindly providing perovskite from the Arkhangelsk kimberlite. Wei-Qiang Ji, Qin Zhou, Zhi-Chao Liu, Chuan-Zhou Liu and Liang-Liang Zhang are thanked for their assistance during sample preparation and analyses. Kevin R. Chamberlain helped to run the TIMS analyses for the AFK perovskite. Constructive reviews by Sebastian Tappe, Anton Chakhmouradian, Keith Bell and Christopher McFarlane improved the manuscript, hence are highly appreciated, as well. This work was supported by the Chinese Academy of Sciences (KZCX2-YW-Q09-15-5) and Natural Science Foundation of China (Grant 41130313) and Russian Foundation for Basic Research (Grant 12-05-00244).

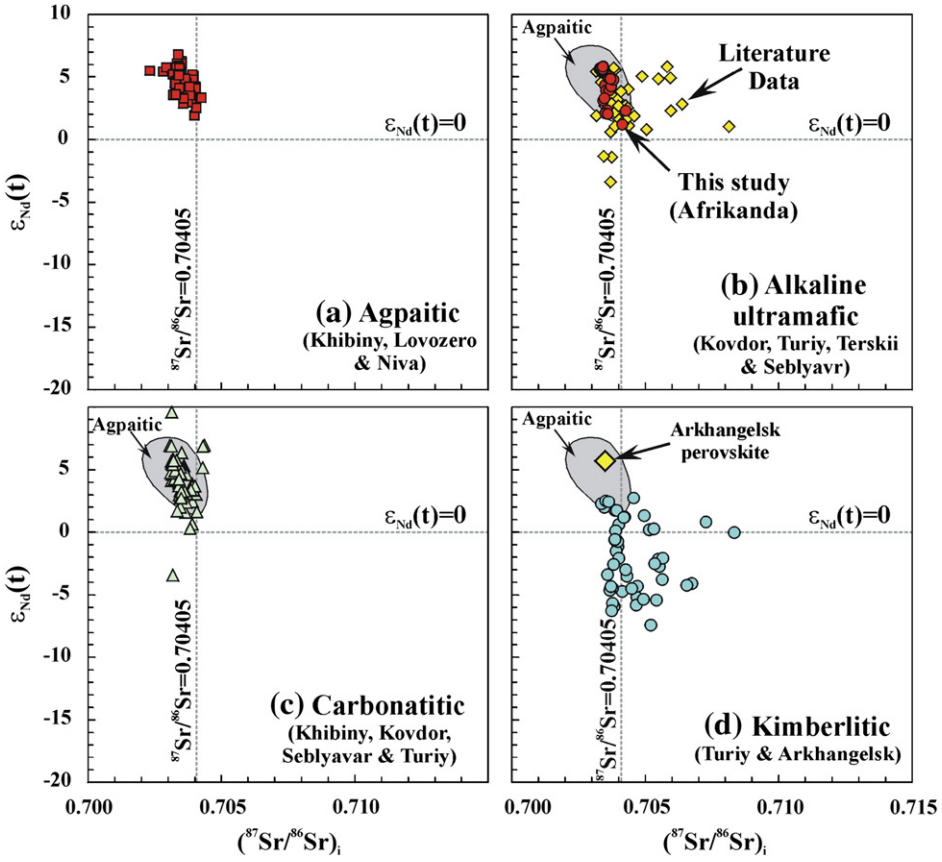

Fig. 12. Sr–Nd isotopic comparisons of the Paleozoic agpaitic (a), ultramafic (b), carbonatitic (c) and "kimberlitic" (d) rocks within the Kola Peninsula.
Data sources: Arzamastsev et al. (2000), Balaganskaya et al. (2007), Beard et al. (1996, 1998, 2000), Dunworth and Bell (2001), Kramm (1994), Kramm and Kogarko (1994), Lee et al. (2006), Mahotkin et al. (2000), Sindern et al. (2004), Verhulst et al. (2000), Wu et al. (2010b, 2010c), Zaitsev and Bell (1995) and Zaitsev et al. (2002).

References

Amelin, Y., Zaitsev, A.N., 2002. Precise geochronology of phoscorites and carbonatites: the critical role of U-series disequilibrium in age interpretations. Geochimica et Cosmochimica Acta 66, 2399–2419.

Arzamastsev, A.A., Belyatsky, B.V., 2000. Palaeozoic activation in the Northeastern Fennoscandian shield: Rb–Sr and Sm–Nd isochron dating of initial volcanics and final dyke pulses of magmatism. Abstracts of the SVEKALAPKO 5th Workshop. Report No. 23. University of Oulu, Department of Geophysics, p. 6.

Arzamastsev, A.A., Glaznev, V.N., 2008. Plume–lithosphere interaction in the presence of an ancient sublithospheric mantle keel: an example from the Kola alkaline province. Doklady Earth Sciences 419A, 384–387.

Arzamastsev, A.A., Mitrofanov, F.P., 2009. Paleozoic plume-lithospheric processes in northeastern Fennoscandia: evaluation of the composition of the parental mantle melts and magma generation conditions. Petrolgy 17, 300–313.

Arzamastsev, A.A., Belyatsky, B.V., Arzamastsev, L.V., 2000. Agpaitic magmatism in the northeastern Baltic Shield: a study of the Niva intrusion, Kola Peninsula, Russia. Lithos 51, 27–46.

Arzamastsev, A.A., Bea, F., Glaznev, V.N., Arzamastseva, L.V., Montero, P., 2001. Kola alkaline province in the Palaeozoic: evaluation of primary mantle magma composition and magma generation conditions. Russian Journal of Earth Sciences 3, 1–32.

Arzamastsev, A.A., Travin, A.V., Belyatskii, B.V., Arzamastseva, L.V., 2003. Paleozoic dike series in the Kola Alkaline Province: age and characteristics of mantle sources. Doklady Earth Sciences 391, 906–909.

Arzamastsev, A.A., Belyatsky, B.V., Travin, A.V., Arzamastsev, L.V., Tsarev, S.E., 2005. Dike rocks in the Khibina massif: relations with the plutonic series, age and characteristics of the mantle source. Petrology 13, 267–288.

Arzamastsev, A.A., Arzamastseva, L.V., Travin, A.V., Belyatsky, B.V., Shamatrina, A.M., Antonov, A.V., Larionov, A.N., Rodionov, N.V., Sergeev, S.A., 2007. Duration of formation of magmatic system of polyphase Paleozoic alkaline complexes of the Central Kola: U–Pb, Rb–Sr, Ar–Ar data. Doklady Earth Sciences 413A, 432–436.

Arzamastsev, A.A., Fedotov, Zh.A., Arzamastseva, L.V., Travin, A.V., 2010. Paleozoic tholeiite magmatism in the Kola igneous province: spatial distribution, ae relations with alkaline magmatism. Doklady Earth Sciences 430, 205–209.

Balaganskaya, E.G., Downes, H., Demaiffe, D., 2007. REE and Sr–Nd isotope compositions of clinopyroxenites, phoscorites and carbonatites of the Seblyavr Massif, Kola Peninsula, Russia. Mineralogia Polonica 38, 29–45.

Balagansky, V.V., Glaznev, V.N., Osipenko, L.N., 1998. Early Proterozoic tectonic evolution of the Kola region, Russia, as revealed by terrane analysis and structural data (in Russian). Geotectonica 2, 16–28.

Bayanova, T.B., 2006. Baddeleyite: a promising geochronometer for alkaline and basic magmatism. Petrology 14, 187–200.

Bayanova, T.B., Levkovich, N.V., Ivanoval, V., 1998. The nature of baddeleyite in different Archean to Paleozoic rocks of the northeastern Baltic Shield. Chinese Science Bulletin 44, A7 (Supp.).

Beard, A.D., Downes, H., Vetrin, V.R., Kempton, P.D., Maluski, H., 1996. Petrogenesis of Devonian lamprophyre and carbonatite minor intrusions, Kandalaksha Gulf Kola Peninsula, Russia. Lithos 39, 93–119.

Beard, A.D., Downes, H., Hegner, E., Sablukov, S.M., Vetrin, V.R., Balogh, K., 1998. Mineralogy and geochemistry of Devonian ultramafic minor intrusions of the southern Kola Peninsula, Russia: implication for the petrogenesis of kimberlites and melilitites. Contributions to Mineralogy and Petrology 130, 288–303.

Beard, A.D., Downes, H., Hegner, E., Sablukov, S.M., 2000. Geochemistry and mineralogy of kimberlites from the Arkhangelsk region, NW Russia: evidence for transitional kimberlite magma types. Lithos 51, 47–73.

Bell, K., 1996. Radiogenic isotope constraints on relationships between carbonatites and associated silicate rocks — a brief review. Journal of Petrology 39, 1987–1996.

Bell, K., Blenkinsop, J., 1987. Archean depleted mantle — evidence from Nd and Sr initial isotope ratios of carbonatites. Geochimica et Cosmochimica Acta 51, 291–298.

Bell, K., Blenkinsop, J., 1989. Neodymium and strontium isotope geochemistry of carbonatites. In: Bell, K. (Ed.), Carbonatites: Genesis and Evolution. Unwin Hyman, London, pp. 278–300.

Bell, K., Rukhlov, A.S., 2004. Carbonatites from the Kola Alkaline Province: origin, evolution and source characteristics. In: Wall, F., Zaitsev, A.N. (Eds.), Phoscorites and Carbonatites from Mantle to Mine: Mineralogical Society Series, 10, pp. 433–468.

Bell, K., Simonetti, A., 2010. Source of parental melts to carbonatites — critical isotopic constraints. Mineralogy and Petrology 98, 77–89.

Brassinnes, S., Balaganskaya, E., Demaiffe, D., 2005. Magmatic evolution of the differentiated ultramafic, alkaline and carbonatite intrusion of Vuoriyarvi (Kola Peninsula, Russia). A LA–ICP–MS study of apatite. Lithos 85, 76–92.

Bulakh, A.G., Nesterov, A.R., Williams, C.T., 2006. Zirconolite, $CaZrTi_2O_7$, re-examined from its type locality at Afrikanda, Kola Peninsula, Russia and some Synroc implications. Neues Jahrbuch für Mineralogie Abhandlungen 182, 109–121.

Burke, K., Roberts, D., Ashwal, L.D., 2007. Alkaline rocks and carbonatites of northwestern Russia and northern Norway: linked Wilson cycle records extending over two billion years. Tectnics 26, TC4015. http://dx.doi.org/10.1029/2006TC002052.

Chakhmouradian, A.R., 2004. Crystal chemistry and paragenesis of compositionally unique (Al-, Fe-, Nb-, and Zr-rich) titanite from Afrikanda, Russia. American Mineralogist 89, 1752–1762.
Chakhmouradian, A.R., Mitchell, R.H., 1997. Compositional variation of perovskite-group minerals from the carbonatite complexes of the Kola Alkaline Province, Russia. The Canadian Mineralogist 35, 1293–1310.
Chakhmouradian, A.R., Mitchell, R.H., 2001a. Occurrence, alteration patterns and compositional variation of perovskite in kimberlites. The Canadian Mineralogist 38, 975–994.
Chakhmouradian, A.R., Mitchell, R.H., 2001b. Three compositional varieties of perovskite from kimberlites of the Lac de Gras field (Northwest Territories, Canada). Mineralogical Magazine 65, 133–148.
Chakhmouradian, A.R., Williams, C.T., 2004. Mineralogy of high-field-strength elements (Ti, Nb, Zr, Ta, Hf) in phoscorititic and carbonatitic rocks of the Kola Peninsula, Russia. In: Wall, F., Zaitsev, A.N. (Eds.), Phoscorites and carbonatites from mantle to mine: The Key Example of the Kola Alkaline Province: Mineralogical Society Series, vol. 10, pp. 293–340.
Chakhmouradian, A.R., Zaitsev, A.N., 1999. Calcite–amphibolite–clinopyroxene rock from the Afrikanda complex, Kola Peninsula, Russia: mineralogy and a possible link to carbonatites. I. Oxide minerals. The Canadian Mineralogist 37, 177–198.
Chakhmouradian, A.R., Zaitsev, A.N., 2002. Calcite–amphibolite–clinopyroxene rock from the Afrikanda complex, Kola Peninsula, Russia: mineralogy and a possible link to carbonatites. III. Silicate minerals. The Canadian Mineralogist 40, 347–1374.
Chakhmouradian, A.R., Zaitsev, A.N., 2004. Afrikanda: an association of ultramafic, alkaline and alkali-silica-rich carbonatitic rocks from mantle-derived melts. In: Wall, F., Zaitsev, A.N. (Eds.), Phoscorites and carbonatites from mantle to mine: The Key Example of the Kola Alkaline Province: Mineralogical Society Series, vol. 10, pp. 247–291.
Chalapathi Rao, N.V., Wu, F.Y., Mitchell, R.H., Li, Q.L., Lehmann, B., 2013. Mesoproterozoic U–Pb ages, trace element and Sr–Nd isotopic composition of perovskite from kimberlites of the Eastern Dharwar craton, southern India: Distinct mantle sources and a widespread 1.1Ga tectonomagmatic event. Chemical Geology 353, 48–64 (this volume).
Chartier, F., Aubert, M., Salmon, M., Tabarant, M., Tran, B.H., 1999. Determination of erbium in nuclear fuels by isotope dilution thermal ionization mass spectrometry and glow discharge mass spectrometry. Journal of Analytical Atomic Spectrometry 14, 1461–1465.
Claesson, S., Vetrin, V., Bayanova, T., Downes, H., 2000. U–Pb zircon ages from a Devonian carbonatite dyke, Kola peninsula, Russia: a record of geological evolution from the Archaean to the Palaeozoic. Lithos 51, 95–108.
Downes, H., Balaganskaya, E., Beard, A., Liferovich, R., Demaiffe, D., 2005. Petrogenetic processes in the ultramafic, alkaline and carbonatitic magmatism in the Kola alkaline province: a review. Lithos 85, 48–75.
Dubois, J.C., Retali, G., Cesario, J., 1992. Isotopic analysis of rare earth elements by total vaporization of samples in thermal ionization mass spectrometry. International Journal of Mass Spectrometry — Ion Process 120, 163–177.
Dunworth, E.A., Bell, K., 2001. The Turiy massif, Kola Peninsula, Russia: isotopic and geochemical evidence for multi-source evolution. Journal of Petrology 42, 377–405.
Ehrlich, S., Gavrieli, I., Dor, L.B., Halicz, L., 2001. Direct high-precision measurements of the $^{87}Sr/^{86}Sr$ isotope ratio in natural water, carbonates and related materials by multiple collector inductively coupled plasma mass spectrometry (MC–ICP–MS). Journal of Analytical Atomic Spectrometry 16, 1389–1392.
Fisher, C.M., McFarlane, C.R.M., Hanchar, J.M., Schmitz, M.D., Sylvester, P.J., Lam, R., Longerich, H.P., 2011. Sm–Nd isotope systematics by laser ablation-multicollector-inductively coupled plasma mass spectrometry: methods and potential natural and synthetic reference materials. Chemical Geology 284, 1–20.
Gorbatschev, R., Bogdanova, S., 1993. Frontiers in the Baltic Shield. Precambrian Research 64, 3–21.
Griffin, W.L., Powell, W.J., Pearson, N.J., O'Reilly, S.Y., 2008. GLITTER: data reduction software for laser ablation ICP–MS. In: Sylvester, P. (Ed.), Laser ablation-ICP-MS in the earth sciences: current practices and outstanding issues: Mineralogical Association Canada Short Course, 40, pp. 308–311.
Harmer, R.E., 1999. The petrogenetic association of carbonatite and alkaline magmatism: constraints from the Spitskop complex, South Africa. Journal of Petrology 40, 525–548.
Heaman, L.M., 2009. The application of U–Pb geochronology to mafic, ultramafic and alkaline rocks: an evaluation of three mineral standards. Chemical Geology 261, 42–51.
Iizuka, T., Eggins, S.M., McCulloch, M.T., Kinsley, L.P.J., Mortimer, G.E., 2011. Precise and accurate determination of $^{147}Sm/^{144}Nd$ and $^{143}Nd/^{144}Nd$ in monazite using laser ablation-MC-ICPMS. Chemical Geology 282, 45–57.
Isnard, H., Brennetot, R., Caussignac, C., Caussignac, N., Chartier, F., 2005. Investigations for determination of Gd and Sm isotopic compositions in spent nuclear fuels samples by MC ICPMS. International Journal of Mass Spectrometry 246, 66–73.
Ivanikov, V.V., Rukhlov, A.S., Bell, K., 1998. Magmatic evolution of the melilitite–carbonatite–nephelinite dyke series of the Turiy peninsula (Kandalaksha Bay, White Sea, Russia). Journal of Petrology 39, 2043–2059.
Jackson, S.E., Pearson, N.J., Griffin, W.L., Belousova, E.A., 2004. The application of laser ablation–inductively coupled plasma–mass spectrometry (LA–ICP–MS) to *in situ* U–Pb zircon geochronology. Chemical Geology 211, 47–69.
Kinny, P.D., Griffin, B.J., Heaman, L.M., Brakhfogel, F.F., Spetsius, Z.V., 1997. SHRIMP U–Pb ages of perovskite from Yakutian kimberlites. Russian Geology and Geophysics 38, 97–105.
Kogarko, L.N., 1987. Alkaline rocks of the eastern part of the Baltic Shield (Kola Peninsula). In: Fitton, J.G., Upton, B.G.J. (Eds.), Alkaline igneous rocks: Geological Society Special Publication, 30, pp. 531–544.
Kogarko, L.N., Kononova, V.A., Orlova, M.P., Wooley, A.R., 1995. Alkaline Rocks and Carbonatites of the World: Part 2: Former USSR. Chapman & Hall, London . 226 pp.
Kramm, U., 1993. Mantle components of carbonatites from the Kola Alkaline Province, Russia and Finland: a Nd–Sr study. European Journal of Mineralogy 5, 985–989.
Kramm, U., 1994. Isotopic evidence for ijolite formation by fenitization: Sr–Nd data of ijolites from the type locality Iivaara, Finland. Contributions to Mineralogy and Petrology 115, 279–286.
Kramm, U., Kogarko, L.N., 1994. Nd and Sr isotope signatures of the Khibina and Lovozero agpaitic centres, Kola Alkaline Province, Russia. Lithos 32, 225–242.
Kramm, U., Kogarko, L.N., Kononova, V.A., Vartiainen, H., 1993. The Kola alkaline province of the CIS and Finland: precise Rb–Sr ages define 380–360 age range for all magmatism. Lithos 30, 33–44.
Kukharenko, A.A., Orlova, M.P., Bulakh, A.G., Bagdasarov, E.A., Rimskaya-Korsakova, O.M., Nefedov, E.I., Ilyinsky, G.A., Sergeev, A.S., Abakumova, N.B., 1965. Caledonian Complex of Ultrabasic, Alkaline Rocks and Carbonatites of the Kola Peninsula and Northern Karelia (in Russia). Nedra, Moscow . 772 pp.
Lee, W.J., Wyllie, P.J., 1998. Petrogenesis of carbonatite magmas from mantle to crust constrained by the system $CaO–(MgO+FeO^*)–(Na_2O+K_2O)–(SiO_2+Al_2O_3+TiO_2)–CO_2$. Journal of Petrology 39, 495–517.
Lee, M.J., Lee, J.I., Hur, S.D., Kim, Y., Moutte, J., Balaganskaya, E., 2006. Sr–Nd–Pb isotopic compositions of the Kovdor phoscorite–carbonatite complex, Kola Peninsula, NW Russia. Lithos 91, 250–261.
Li, X.H., Liu, Y., Li, Q.L., Guo, C.H., Chamberlain, K.R., 2009. Precise determination of Phanerozoic zircon Pb/Pb age by multi-collector SIMS without external standardization. Geochemistry, Geophysics, Geosystem. http://dx.doi.org/10.1029/2009GC00 2400.
Li, Q.L., Li, X.H., Liu, Y., Wu, F.Y., Yang, J.H., Mitchell, R.H., 2010. Precise U–Pb and Th–Pb age determination of kimberlitic perovskites by secondary ion mass spectrometry. Chemical Geology 269, 396–405.
Ludwig, K.R., 2003. ISOPLOT 3.0—a geochronological toolkit for Microsoft Excel. Berkeley Geochronology Center Special Publication, No. 4 . 70 pp.
Mahotkin, I.L., Gibson, S.A., Thompson, R.N., Zhuravlev, D.Z., Zherdev, P.U., 2000. Late Devonian diamondiferous kimberlite and alkaline picrite (proto-kimberlite?) magmatism in the Arkhangelsk region, NW Russia. Journal of Petrology 41, 201–227.
Marty, B., Tolstikhin, I., Kamensky, I.L., Nivin, V., Balaganskaya, E., Zimmermann, J.L., 1998. Plume-derived rare gases in 380 Ma carbonatites from the Kola region (Russian) and the argon isotopic composition in the deep mantle. Earth and Planetary Science Letters 164, 179–192.
Matukov, D.I., Lepekhina, E.N., Bagdasarov, E.A., Antonov, A.V., Sergeev, S.A., 2006. SHRIMP-II U–Pb dating of perovskite from ultramafic alkaline intrusion. Geochimica et Cosmochimica Acta 70, A402 (supplement).
McFarlane, C.R.M., McCulloch, M.T., 2007. Coupling of in-situ Sm–Nd systematics and U–Pb dating of monazite and allanite with applications to crustal evolution studies. Chemical Geology 245, 45–60.
Menzies, M., 1987. Alkaline rocks and their inclusions: a window on the Earth's interior. In: Fitton, J.G., Upton, B.G.J. (Eds.), Alkaline Igneous Rocks. Geological Society Special Publication 30, pp. 15–27.
Mitchell, R.H., 2005. Carbonatites and carbonatites and carbonatites. The Canadian Mineralogist 43, 2049–2068.
Mitchell, R.H., 2006. Potassic magmas derived from metasomatized lithospheric mantle: nomenclature and relevance to explanation for diamond bearing rocks. Journal Geological Society of India 67, 317–327.
Mitchell, R.H., Wu, F.Y., Yang, Y.H., 2011. In situ U–Pb, Sr and Nd isotopic analysis of loparite by LA–(MC)–ICP–MS. Chemical Geology 280, 191–199.
Mitrofanov, F.P., 2001. Modern problems and some solutions of the Precambrian Geology of Cratons (in Russian). Litosfera 1, 5–14.
Oversby, V.M., Ringwood, A.E., 1981. Lead isotopic studies of zirconolite and perovskite and their implications for long range Synroc stability. Radioactive Waste Management 1, 289–307.
Peltonen, P., Brugmann, G., 2006. Origin of layered continental mantle (Karelian craton, Finland): geochemical and Re–Os isotope constraints. Lithos 89, 405–423.
Pozhilenko, V.I., Gavrilenko, B.V., Zhirov, D.V., Zhabin, S.V., 2002. Geology of the Ore Regions of the Murmansk region (in Russian). Apatity, Kola Science Centre Publications. 359 pp.
Ramos, F.C., Wolff, J.A., Tollstrup, D.L., 2004. Measuring $^{87}Sr/^{86}Sr$ variation in minerals and groundmass from basalts using LA–MC–ICPMS. Chemical Geology 211, 135–158.
Reguir, E.P., Camacho, A., Yang, P., Chakhmouradian, A.R., Kamenetsky, V.S., Halden, N.M., 2010. Trace-element study and uranium-lead dating of perovskite from the Afrikanda plutonic complex, Kola Peninsula (Russia) using LA–ICP–MS. Mineralogy and Petrology 100, 95–103.
Rodionov, N.V., Belyatsky, B.V., Antonov, A.V., Kapitonov, I.N., Sergeev, S.A., 2012. Comparative in-situ U–Th–Pb geochronology and trace element composition of baddeleyite and low-U zircon from carbonatites of the Palaeozoic Kovdor alkaline–ultramafic complex, Kola Peninsula, Russia. Gondwana Research 21, 728–744.
Rukhlov, A.S., Bell, K., 2010. Geochronology of carbonatites from the Canadian and Baltic shields, and the Canadian Cordillera: clues to mantle evolution. Mineralogy and Petrology 98, 11–54.
Simonetti, A., Bell, K., 1994a. Nd, Pb and Sr isotopic data from the Napak carbonatite–nephelinite centre, eastern Uganda: an example of open-system crystal fractionation. Contributions to Mineralogy and Petrology 115, 356–366.
Simonetti, A., Bell, K., 1994b. Isotopic and geochemical investigation of the Chilwa Island carbonatite complex, Malawi: evidence for a depleted mantle source region, liquid immiscibility, and open-system behaviour. Journal of Petrology 35, 1597–1621.
Simonetti, A., Goldstein, S.L., Schmidberger, S.S., Viladkar, S.G., 1997. Geochemical and Nd, Pb, and Sr isotope data from deccan alkaline complexes — inferences for mantle sources and plume–lithosphere interaction. Journal of Petrology 39, 1847–1864.
Sindern, S., Zaitsev, A.N., Demény, A., Bell, K., Chakmouradian, A.R., Kramm, U., Moutte, J., Rukhlov, A.S., 2004. Mineralogy and geochemistry of silicate dyke rocks associated with carbonatites from the Khibina complex (Kola, Russia) — isotope constraints on genesis and small-scale mantle sources. Mineralogy and Petrology 80, 215–239.

Sørensen, H., 1974. The Alkaline Rocks. John Wiley & Sons, London . 622 pp.
Stacey, J.S., Kramers, J.D., 1975. Approximation of terrestrial lead isotope evolution by a two-stage model. Earth and Planetary Science Letters 26, 207–221.
Tappe, S., Simonetti, A., 2012. Combined U–Pb geochronology and Sr–Nd isotope analysis of the Ice River perovskite standard, with implications for kimberlite and alkaline rock petrogenesis. Chemical Geology 304 (305), 10–17.
Tappe, S., Foley, S.F., Jenner, G.A., Kjarsgaard, B.A., 2005. Integrating ultramafic lamprophyres into the IUGS classification of igneous rocks: rational and implications. Journal of Petrology 46, 1893–1900.
Tappe, S., Foley, S.F., Stracke, A., Romer, R.L., Kjarsgaard, B.A., Heaman, L.M., Joyce, N., 2007. Craton reactivation on the Labrador Sea margins: $^{40}Ar/^{39}Ar$ age and Sr–Nd–Hf–Pb isotope constraints from alkaline and carbonatite intrusives. Earth and Planetary Science Letters 256, 433–454.
Tolstikhin, I.N., Kamensky, I.L., Marty, B., Nivin, V.A., Vetrin, V.R., Balaganskaya, E.G., Ikorsky, S.V., Gannibal, M.A., Weiss, D., Verhulst, A., Demaiffe, D., 2002. Gas, rare isotopes and parent trace elements in ultrabasic–alkaline–carbonatite complexes, Kola Peninsula: identification of lower mantle plume component. Geochimica et Cosmochimica Acta 66, 881–901.
Verhulst, A., Balaganskaya, E., Kirnarsky, Y., Demaiffe, D., 2000. Petrological and geochemical (trace elements and Sr–Nd isotopes) characteristics of the Paleozoic Kovdor ultramafic, alkaline and carbonatite intrusion (Kola Peninsula, NW Russia). Lithos 51, 1–25.
Vervoort, J.D., Patchett, P.J., Soderlund, U., Baker, M., 2004. Isotopic composition of Yb and the determination of Lu concentrations and Lu/Hf ratios by isotopic dilution using MC–ICPMS. Geochemistry, Geophysics, Geosystems (G3) 5, Q11002. http://dx.doi.org/10.1029/2004GC000721.
Waight, T., Baker, J., Willigers, B., 2002. Rb isotope dilution analyses by MC–ICPMS using Zr to correct for mass fractionation: towards improved Rb–Sr geochronology? Chemical Geology 186, 99–116.
Wasserburg, G.J., Jacobsen, S.B., DePaolo, D.J., McCulloch, M.T., Wen, T., 1981. Precise determination of Sm/Nd ratios, Sm and Nd isotopic abundances in standard solutions. Geochimica et Cosmochimica Acta 45, 2311–2323.
Williams, I.S., 1998. U–Th–Pb geochronology by ion microprobe. In: McKibben, M.A., Shanks III, W.C., Ridley, W.I. (Eds.), Applications of microanalytical techniques to understanding mineralizing processes: Reviews in Economic Geology, 7, pp. 1–35.
Williams, C.T., Gieré, R., 1996. Zirconolite: a review of localities worldwide, and a compilation of its chemical compositions. Bulletin of the Natural History Museum, London (Geology) 52, 1–24.
Williams, C.T., Bulakh, A.G., Gieré, R., Lumpkin, G.R., Mariano, A.N., 2001. Alteration features in natural zirconolite from carbonatites. In: Hart, K.P., Lumpkin, G.R. (Eds.), Material Research Society: Symposium Proceedings, 663, pp. 945–952.
Woolley, A.R., Kjarsgaard, B.A., 2008. Paragenetic types of carbonatite as indicated by the diversity and relative abundances of associated silicate rocks: evidence from a global database. The Canadian Mineralogist 46, 741–752.
Wu, F.Y., Yang, Y.H., Xie, L.W., Yang, J.H., Xu, P., 2006. Hf isotopic compositions of the standard zircons and baddeleyites used in U–Pb geochronology. Chemical Geology 234, 105–126.
Wu, F.Y., Yang, Y.H., Mitchell, R.H., Li, Q.L., Yang, J.H., Zhang, Y.B., 2010a. *In situ* U–Pb age determination and Nd isotopic analyses of perovskites from kimberlites in southern Africa and Somerset Island, Canada. Lithos 115, 205–222.
Wu, F.Y., Yang, Y.H., Marks, M.A.W., Liu, Z.C., Zhou, Q., Ge, W.C., Yang, J.S., Zhao, Z.F., Mitchell, R.H., Markl, G., 2010b. *In situ* U–Pb, Sr, Nd, and Hf isotopic analysis of eudialyte by LA–(MC)–ICP–MS. Chemical Geology 273, 8–34.
Wu, F.Y., Yang, Y.H., Mitchell, R.H., Bellatreccia, F., Li, Q.L., Zhao, Z.F., 2010c. *In situ* U–Pb and Nd–Hf–(Sr) isotopic investigations of zirconolite and calzirtite. Chemical Geology 277, 178–195.
Wu, F.Y., Mitchell, R.H., Li, Q.L., Sun, J., Liu, C.Z., Yang, Y.H., 2013. In situ U–Pb age determination and Sr–Nd isotopic analyses of perovskite from the Premier (Cullinan) kimberlite, South Africa. Chemical Geology 353, 83–95 (this volume).
Xie, L.W., Zhang, Y.B., Zhang, H.H., Sun, J.F., Wu, F.Y., 2008. In situ simultaneous determination of trace elements, U–Pb and Lu–Hf isotopes in zircon and baddeleyite. Chinese Science Bulletin 53, 1565–1573.
Yang, Y.H., Sun, J.F., Xie, L.W., Fan, H.R., Wu, F.Y., 2008. In situ Nd isotopic measurements of geological samples by laser ablation. Chinese Science Bulletin 53, 1062–1070.
Yang, Y.H., Wu, F.Y., Wilde, S.A., Liu, X.M., Zhang, Y.B., Xie, L.W., Yang, J.H., 2009. In situ perovskite Sr–Nd isotopic constraints on petrogenesis of the Mengyin kimberlites in the North China Craton. Chemical Geology 264, 24–42.
Zaitsev, A., Bell, K., 1995. Sr and Nd isotope data of apatite, calcite and dolomite as indicators of source, and the relationships of phoscorites and carbonatites from the Kovdor massif, Kola Peninsula, Russia. Contributions to Mineralogy and Petrology 121, 324–335.
Zaitsev, A.N., Chakhmouradian, A.R., 2002. Calcite–amphibolite–clinopyroxene rock from the Afrikanda complex, Kola Peninsula, Russia: mineralogy and a possible link to carbonatites. II. Oxysalt minerals. The Canadian Mineralogist 40, 103–120.
Zaitsev, A.N., Demény, A., Sindern, S., Wall, F., 2002. Burbankite group minerals and their alteration in rare earth carbonatites-source of elements and fluids (evidence from C–O and Sr–Nd isotopic data). Lithos 62, 15–33.
Zaitsev, A.N., Sitnikova, M.A., Subbotin, V.V., Fernandes-Suarez, J., Jeffries, T.E., 2004. Sallanlatvi complex—a rare example of magnesite and siderite carbonatites. In: Wall, F., Zaitsev, A.N. (Eds.), Phoscorites and Carbonatites from Mantle to Mine: Mineralogical Society Series, 10, pp. 201–246.